TAMPEREEN TEKNILLINEN YLIOPISTO
TAMPERE UNIVERSITY OF TECHNOLOGY

JOONA UUSITALO

NOVEL SENSOR SOLUTIONS WITH APPLICATIONS TO MONITORING OF ELEVATOR SYSTEMS

Master of Science Thesis

Examiner: Dr. Tomi Krogerus,
Prof. Jukka Vanhala
Examiners and topic approved on 1 November 2017

ABSTRACT

JOONA UUSITALO: Novel Sensor Solutions with Applications to Monitoring of Elevator Systems
Tampere University of technology
Master of Science Thesis, 50 pages, 20 Appendix pages
February 2018
Master's Degree Programme in Electrical Engineering
Major: Electronics
Examiner: Doctor Tomi Krogerus, Professor Jukka Vanhala

Keywords: sensor system, condition monitoring, positioning

The task of this master's thesis was to design and implement a mobile and easy to use sensor system to monitor elevator systems. This sensor system would be used to collect data for research use. The sensor system should be capable to monitor the movement of the elevator car and environmental values of the elevator system. In addition to storing measured data locally, the sensor system should be also capable to store the measured data to a cloud server. Other task was to research a method to determine the position of the elevator car in the elevator shaft.

Raspberry Pi 3 Model B is the base of the designed prototype. All the used sensors are in TI's plug-in module, which connects to the Raspberry via I2C. The module includes accelerometer, gyroscope, magnetometer, air pressure sensor, humidity sensor and temperature sensor. To determine the position of the elevator car, the prototype utilizes Marvelmind indoor navigation system. The mobile beacon of the Marvelmind system connects via USB to the Raspberry. The prototype connects wirelessly to TUT-wireless network enabling saving data to a cloud server. The prototype measures the inertial movements with sampling frequency of 400 Hz and environmental values with 40 Hz.

The overall performance of the prototype was tested in real elevator systems while the performance of the positioning accuracy was tested in simulated elevator system in the corridor of Konetalo. The results from the tests in real elevator systems showed that the prototype obtains and stores the data correctly. The results from the tests in simulated elevator system showed that the Marvelmind system can be used to determine the position of the elevator car in the elevator shaft with some restriction.

TIIVISTELMÄ

JOONA UUSITALO: Uudet anturiratkaisut hissijärjestelmien monitorointisovelluksissa
Tampereen teknillinen yliopisto
Diplomityö, 50 sivua, 20 liitesivua
Helmikuu 2018
Sähkötekniikan diplomi-insinöörin tutkinto-ohjelma
Pääaine: Elektroniikka
Tarkastaja: tohtori Tomi Krogerus, professori Jukka Vanhala

Avainsanat: anturijärjestelmä, kunnonvalvonta, paikannus

Tämän diplomityön tavoitteena oli suunnitella ja toteuttaa liikuteltava ja helposti käytettävä anturijärjestelmä hissijärjestelmien valvontaan. Tätä anturijärjestelmää käytettäisiin datan keräämiseen tutkimustarkoitukseen. Anturijärjestelmän tulisi kyetä valvomaan hissikorin liikkeitä ja hissijärjestelmän ympäristöarvoja. Mitatun datan paikallisen tallentamisen lisäksi anturijärjestelmän tulisi kyetä tallentamaan mitattu data pilvipalvelimelle. Toinen tavoite oli tutkia menetelmää hissikorin sijainnin määrittämiseksi hissikuilussa.

Raspberry Pi 3 Model B on suunnitellun prototyypin perusta. Kaikki käytetyt anturit ovat TI:n plug-in moduulissa, joka yhdistyy Raspberryyn I2C:n kautta. Moduuli sisältää kiihtyvyysanturin, gyroskoopin, magnetometrin, ilmanpaineanturin, kosteusanturin ja lämpötila-anturin. Hissikorin sijainnin määrittämiseen prototyyppi käyttää Marvelmindin sisäpaikannusjärjestelmää. Marvelmindin järjestelmän mobiilimajakka liittyy Rasbperryyn USB:n kautta. Prototyyppi yhdistyy langattomasti TUT-langattomaan verkkoon mahdollistaen datan tallentamisen pilvipalvelimelle. Prototyyppi mittaa inertialiikkeitä 400 Hz näytteenottotaajuudella ja ympäristöarvoja 40 Hz.

Prototyypin yleissuorituskykyä testattiin oikeissa hissijärjestelmissä, kun taas sijainnin tarkkuuden määrittämisen suorituskyky testattiin Konetalon käytävälle simuloidussa hissijärjestelmässä. Oikeissa hissijärjestelmissä suoritettujen testien tulokset osoittavat, että prototyyppi mittaa ja tallentaa datan oikein. Simuloidussa hissijärjestelmässä suoritettujen testien tulokset osoittavat, että Marvelmindin järjestelmää voidaan käyttää hissikorin sijainnin määrittämiseen hissikuilussa tietyin rajoituksin.

PREFACE

This thesis was part of a research project called OPENS and done for the Laboratory of Intelligent Hydraulics of Tampere University of Technology. This thesis concludes my studies at Tampere University of Technology. Tampere has served me well during these years and now it is time to move on to new challenges in next destination.

First, I want to thank Tomi Krogerus for giving me these opportunity and subject for Master's thesis. He has been great and upstanding boss and examiner during this thesis. I want also to thank my other examiner, Jukka Vanhala, for giving advices and help for this thesis.

Second, I want to thank my girlfriend, Vilma, and my family for all the support during my studies and life in Tampere. I want also to thank my friends and schoolmates for being great friends and occasionally offering peer support during my studies.

Tampere 31.12.2017

Joona Uusitalo

CONTENTS

LIST OF SYMBOLS AND ABBREVIATIONS

AGC	Automatic Gain Control
AMR	Anisotropic Magneto-Resistance
CPU	Central Processing Unit
CSV	Comma-Separated Values
DSI	Display Serial Interface
G-force	Gravitational force
GMN	Earth's Geomagnetic Noise
GPIO	General-Purpose Input/Output
GPU	Graphics Processing Unit
HDMI	High Definition Multimedia Interface
I2C	Inter-Integrated Circuit
IMU	Inertial Measurement Unit
INS	Inertial Navigation System
IoT	Internet of Things
IP	Internet Protocol
ISM	Industrial, Scientific and Medical
LED	Light-Emitting Diode
LIDAR	Light Detection and Ranging
MEMS	Microelectromechanical System
NMEA	The National Marine Electronics Association
PC	Personal Computer
R2R	Roll-to-roll Printing Technology
RAM	Random Access Memory
RH	Relative Humidity
SoC	System-on-Chip
SONAR	Sound Navigation and Ranging
SPI	Serial Peripheral Interface
SSH	Secure Shell
TI	Texas Instruments
TOF	Time-of-Flight
TUT	Tampere University of Technology
UART	Universal Asynchronous Receiver-Transmitter
USB	Universal Serial Bus
WLAN	Wireless Local Area Network

1. INTRODUCTION

During the las years, the significance of reliability and high availability of machine systems have been strongly emphasized [1]. Because of this, service operations have nowadays a major role in the business of machine manufacturing companies. While service operations today are often based on regular maintenance, there is fast-growing interest in smarter solutions. These smarter solutions will be used to both diagnose and predict the future operation and condition of machine systems. A modern complex machine system can have hundreds of moving parts that need regular checks and maintenance. Thus, a huge potential in predictive maintenance frameworks exists for optimizing the current and future maintenance actions.

Predictive maintenance strategies depend heavily on the collected data from the monitored machine systems. Therefore, sensors play a key role in advanced solutions being the artificial "eyes and ears" of machine systems capturing the information about the current condition and performance [2]. In this thesis, elevator systems are selected as our machine systems where sensor solutions are studied.

To build data models for predictive maintenance, we need lot of data from various situations like normal operation and abnormal actions. The main task of this thesis is to build a prototype sensor system to collect data from different elevators for analytics and machine learning. For practical reasons, it is not within the scope of this thesis to utilize the information of the elevator control system. Thus, the prototype should only rely on its own sensors and transducers to do the measurements and the monitoring of the elevator system.

A transducer is a device that converts energy from one form into another form [3]. A sensor is a form of transducer. It detects or measures a physical quantity as an input and converts it to an electrical output. The input is some type of phenomena from physical environment. This phenomenon can be light, heat, motion, moisture, pressure, magnetism or any other environmental phenomena. The output from a sensor needs to behave to the sensed phenomena relatively or at least according to some mathematical relationship so that measuring and calibration would be possible. The resolution of a sensor stands for the smallest change that sensor can detect.

In the past sensors were based on many different systems but nowadays microelectromechanical systems (MEMS) have replaced these [4]. This is due to reason that MEMS sensors are smaller and cheaper to manufacture. For example, piezoelectric sensors are man-

ufactured traditionally one device at the time whereas MEMS sensors utilize batch fabrication process enabling simultaneous processing of thousands of identical devices on single wafer. Economical MEMS sensors have widened sensor markets in both technology industry and consumer markets and enabled manufacturing of completely new devices.

While the technology of MEMS sensors is suitable for measuring physical variables, it is less suitable for chemical and gas sensing applications [5]. This is due to reason that we have not yet discovered a suitable "silicon" substrate for chemical sensors that meets the requirements for high-volume fabrication. The markets, which have great demand for chemical and gas sensing applications, are in healthcare, the food industry, farming and environmental monitoring. The solution for the fabrication problem could be in roll-to-toll (R2R) technology, which makes possible of manufacturing billions of disposable chemical sensors with low cost [5]. This technology could also provide the solution for the physical sensors facing their limits in miniaturization.

The global sensor market has been expanding constantly during the past years. Nowadays we install sensors everywhere. Sensor use in consumer markets increased significantly in year 2007 when the presentation of the iPhone and the Wii gaming platform occurred [5]. Today smartphones contain so many sensors that they can sense motion, temperature, pressure, sound, light, humidity, touch, magnetism and other physical phenomena. Most of the present cars contain even more sensors [5]. The number of sensors installed to present cars varies from several tens to around 100. The development of self-driving cars is increasing even more the sensor use in cars. The healthcare sector is also turning out to be a big and potential market [5]. The market for disposable medical sensors has proved to be significant and the treatment of chronic diseases could create a trillion sensor market. The highly topical Internet of Things (IoT) is growing to be big thing in the future as well. Many believe that most of the devices connected in the IoT will be embedded sensors [5]. IoT sensor business has markets in home automation, commercial building automation, media and gaming, healthcare, the industrial internet and transportation.

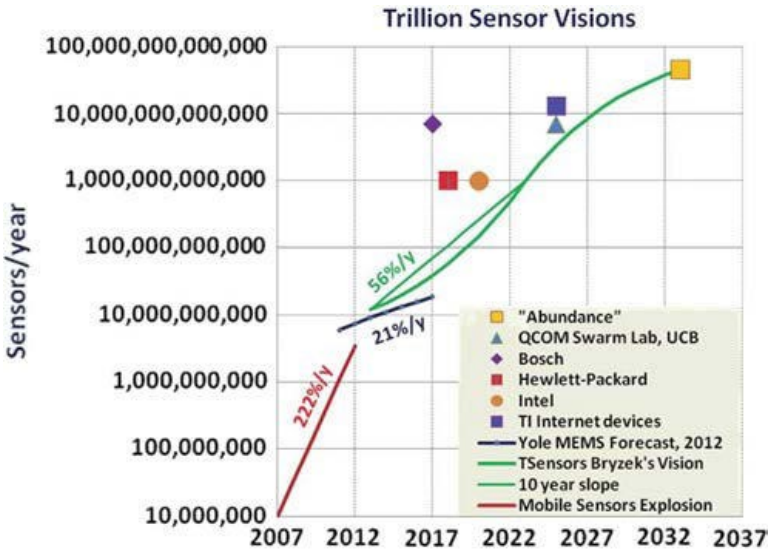

Figure 1. *Actual and predicted growth in the global sensor market [5].*

Figure 1 demonstrates how rapid the growth in sensor markets has been after year 2007. The predicted growth and several visionary organizations predict that the sensor markets will hit one trillion mark around 2022-2027. The increasing demand for sensors is changing our lives and the way we design and operate devices.

This thesis consists of five chapters. The second chapter represents sensor solutions of elevator monitoring. It illustrates what kind of possibilities IoT provides, what kind of variables the prototype needs to monitor, how the sensors work and what kind of commercial monitoring systems are already in the market. The third chapter introduces the developed prototype and the components utilized in the prototype. Furthermore, it explains how the software of the prototype works and how it handles the measured data. The fourth chapter presents the conducted tests and both the results and all the other major observations from the tests. The final fifth chapter gives a brief summary and a conclusion to this master's thesis. It also considers the performance and the successfulness of the prototype and the possible future improvements.

2. SENSOR AND MONITORING SOLUTIONS IN ELEVATOR SYSTEMS

The main idea behind predictive maintenance is to prevent unexpected equipment failures by monitoring the equipment and perform maintenance when the maintenance activity is most cost-effective and before the equipment loses performance. Doing this reduces unplanned downtime costs caused by failures. Predictive maintenance relies on analyzed sensor data collected from the machine system. Predictive maintenance is currently a hot topic in many fields e.g. automotive and airline industry, heavy equipment etc. [1].

In this thesis, elevator systems have been selected as a research platform to conduct our studies of development of novel sensor system for mobile machine systems. Nowadays over half of the World's population lives in urban areas, which induces logistical challenges not only in horizontal transportation but also in vertical transportation otherwise known as elevators [6]. The number of elevators in just Europe is over 4.3 million. Usually one elevator can be in service for 25 years or longer before a major modernization. Due to more and more advancing technology, people demand more and more comfortable and safe elevator transportation [7]. Usually small vibration during elevator ride is not enough to cause discomfort to passengers. After the vibration reaches certain value, passengers will feel great discomfort, which causes them to feel unsafe in the elevator. To identify the sources of vibrations and other phenomena causing discomfort, elevator systems need sensor systems that collect data of all the physical actions during the elevator ride. From the data, we can then discover the reasons for uncomfortable rides.

To adapt to the increasing transportation demands of the future, the elevator companies have come to realize that they need to change their maintenance strategies from preventative and corrective to predictive and preemptive [6]. These new maintenance strategies could help to schedule services at times with minimum of interference and maximize the system's uptime. Most of the state of the art elevator systems have various sensors preinstalled and are connected to the cloud [6]. They can collect and process the data from the elevator sensors to produce information about the elevator system's health state and potential future problems and maintenance targets. However, old elevators do not support this kind of maintenance strategies. For this purpose, Skog et al. state that elevator industry needs novel sensor solutions with applications to monitoring of elevator systems that are easy to install to existing elevators [6].

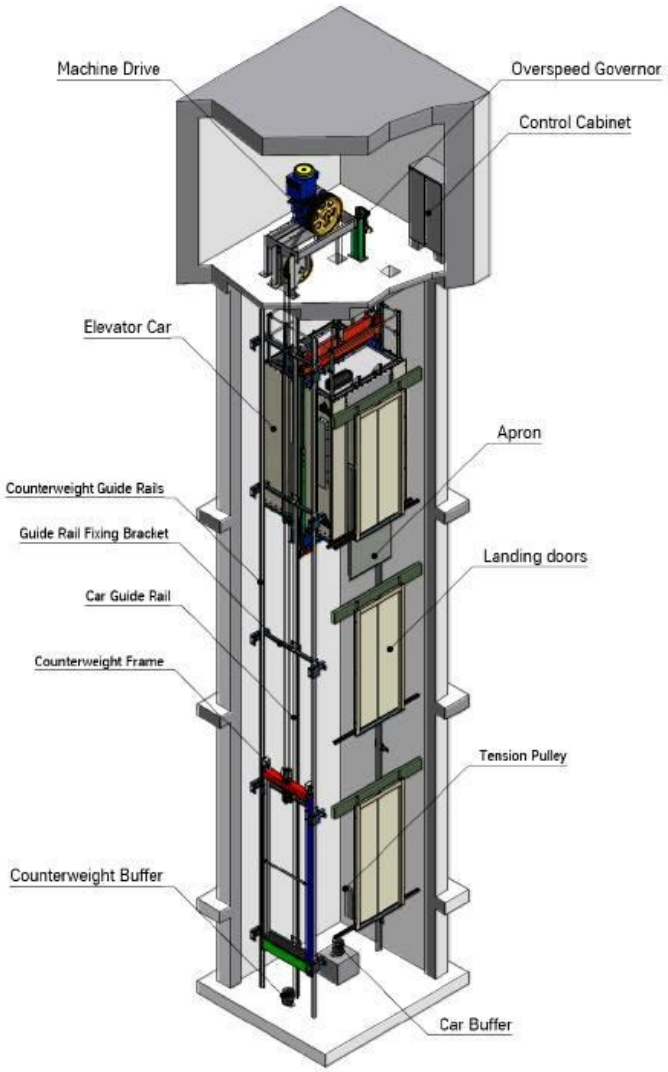

Figure 2. *A basic elevator system [8].*

Figure 2 presents a basic elevator system. The main task of the elevator is to transport an elevator car between different floor levels. Most of the commercial elevators use an engine to drive a traction cable system to do this [6, 8]. In heavy-duty elevators, hydraulic system replaces the traction cable system. The car slides against the guide rails with guide shoes or rollers, which maintain the horizontal position of the car. Modern elevator systems usually have a motorized or semi-motorized door system, which provides protection to the passengers during the elevator ride.

To monitor elevator systems, the sensor system would need to be installed to the elevator car and have various sensors with which it captures all the physical happenings in operating elevator [6]. In the envisioned sensor system by Skog et al., a cloud server receives the measured data from the sensor system and analyzes it [6]. The cloud server combines the data with previous data and historical maintenance statistics to determine the maintenance strategy. If the elevator needs maintenance, the maintenance strategy informs a service technician about it who receives the cause for maintenance and services to carry

out. After the maintenance, the service technician reports back to the cloud about the adjustments and repairs made.

Elevator monitoring systems usually utilize either model-based or data-driven condition monitoring technique [6]. The model-based technique does not need any training data but needs prior knowledge of elevator system specific parameters. On the contrary, the data-driven technique does not need any elevator specific parameters but it instead needs large amounts of training data. Due to number of different elevators on the market, large-scale deployment of condition monitoring systems utilizing the model-based technique is impracticable. Then again, acquiring the training data from prior elevator systems and faults is time consuming and costly.

It is not enough that we only gather data but we also need a method to transmit the data to the cloud server. Nowadays, the simplest method is to transmit it over the internet [6, 9]. If the cloud server receives the data via cellular network, cellular data fees will limit the amount of the data that is financially reasonable. This creates a challenge what amount of data is enough for data mining and machine learning in the cloud server. One solution is that the sensor node either compresses the measured data or extracts only the essential information from the measured data and sends it to the cloud. This again creates a challenge what is the essential information or can we compress the data without losing important information.

To know what sensors the sensor node needs we have to identify first what we want to measure. We need to have data about the behavior of the elevator during the normal operation like a travel pattern, usage statistics, acceleration and speed statistics and environmental values [6]. The most common faults of elevator systems are the abnormal behavior of the doors of an elevator car, both abnormal noises and jerks during operation, emergency stops, the floor of the elevator car not lining up with the floor of the building and wearing of different components such as engine bearings, guide shoes, guide rollers, guide rails and wire rope [6, 7, 9-11]. Large changes in environmental values can cause unpredicted strain to these components. Most of the listed faults cause abnormal behavior to vibration and motion of the elevator car. Thus, the sensor node should be able to sense motion and environmental phenomena.

2.1 Motion sensing

Inertial sensors measure a physical phenomenon called inertial force or familiarly motion [12]. Usually these sensors transduce the force into a linearly scaled voltage output with a defined sensitivity. The two most important and used inertial sensors are an accelerometer and a gyroscope [13]. An inertial measurement unit (IMU) usually measures both acceleration with three orthogonal accelerometers and the rate of change of the orientation with three orthogonal gyroscope. This way enables IMU to capture acceleration and the rate of change of the orientation in all three dimensions.

Accelerometers are one of the most sold MEMS sensors worldwide [4]. One reason for this is the automotive industry. Most cars use high G-forces (gravitational forces) sensing accelerometers for air bag deployment. In addition to that some cars use low G-forces sensing accelerometers for active suspension and vehicle stabilization control. Mobile machines can also use accelerometers to measure speed and traveled distance [3]. We can find the change of speed with mathematical action by integrating the acceleration with regard to time and the travelled distance by integrating the speed with regard to the time.

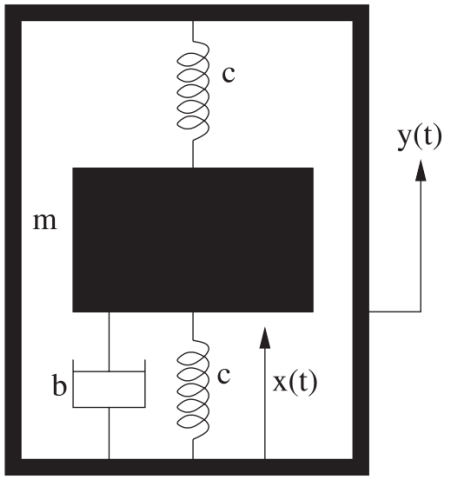

Figure 3. *The principle of single-axis accelerometer [13].*

Figure 3 presents the basic structure of accelerometer. This structure consists of an elastic element of stiffness *c* that suspends a proof mass *m to* the frame [4, 13]. The proof mass will fall behind the frame motion $y(t)$ because of the mass inertia, which causes the displacement of the proof mass $x(t)$. Installing a viscous damper *b* counteracts this excessive ringing and damps vibration. The equation (1) below expresses the dynamics of this system.

$$\ddot{x}(t) + 2\zeta\omega_n\dot{x}(t) + \omega_n^2 x(t) = -\ddot{y}(t) \quad (1)$$

Equation (1) describes how acceleration of the sensor body $\ddot{y}(t)$ converts to displacement $x(t)$ with a natural frequency ω_n and a damping ratio ζ. The parameters *b, m* and *c* affect the resonance that usually is set much higher than the motion frequency range [13].

Accelerometers can measure either in single axis or in multiple axis depending on the designed structure of the sensor. It is possible to measure acceleration on three axis with a single proof mass [4]. In this case, the accelerometer measures the mass displacement in all three directions from which it deduces the acceleration. However, most of the accelerometers measure three-axis acceleration with multiple independent proof masses.

There are currently three sensing principles for MEMS accelerometers: capacitive, piezoelectric and piezoresistive [4, 13]. Capacitive sensing detects small changes in capacitance caused by the relative movement of the proof mass and the frame. In piezoelectric

sensing, the inertial force causes strain on piezoelectric material that generates a charge polarization. In a simple structure, a piezoelectric plate acts as a spring and connects the proof mass. The current generated in the piezoelectric plate is relative to the change in acceleration. Piezoelectric sensors have large dynamic range but cannot sense dc-acceleration. Piezoresistive sensing integrates piezoresistors to the spring. When acceleration induces stress to the spring the piezoresistor resistance changes from which it deduces acceleration. Piezoresistive sensors are durable but have poor noise and power performance. Currently the most used accelerometers use capacitive sensing as they have good noise and power performance and are inexpensive.

Gyroscopes measure how quickly an object turns [4]. Other names for gyroscopes are an angular velocity sensor and a rotation rate sensor. Optical gyroscopes provide the most accurate measurements and withstand a mechanical wear [4]. These gyroscopes measure the phase difference of two laser beams travelling in opposing directions. The downside of optical gyroscopes are their large size and high price. MEMS gyroscope provide answer to this problem being lightweight, small and inexpensive. They utilize capacitive sensing and actuation in measurements. Of all the MEMS sensors gyroscopes are the most complicated sensors due to the primary reason that the Coriolis force is very small.

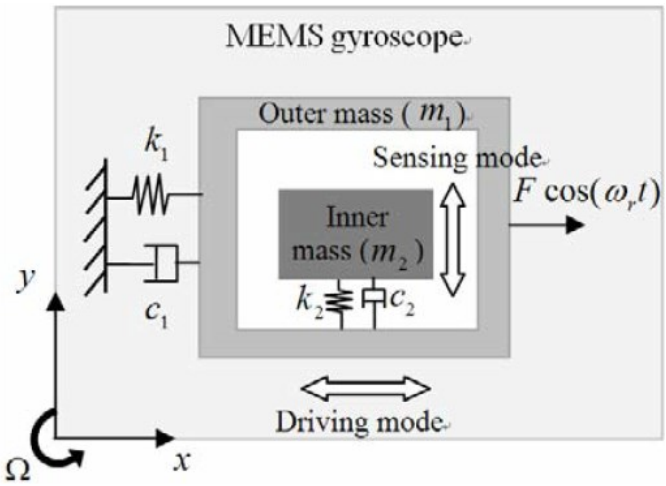

Figure 4. *The principle of vibrating two-mode gyroscope [14].*

Figure 4 illustrates the basic structure of vibrating two-mode gyroscope, which major of MEMS gyroscopes are. This structure consists of an outer mass m_1, an inner mass m_2, an outer beam spring k_1, an inner beam spring k_2, a driving direction damping coefficient c_1 and a sensing direction damping coefficient c_2 [4, 14]. The driving mode is orthogonal to the sensing mode. This eliminates the interference between these modes. If the MEMS gyroscope does not rotate around z-axis, there is no Coriolis force and both inner and outer mass vibrate only along x-axis in driving mode. When the MEMS gyroscope rotates around z-axis with an angular rate Ω, it produces Coriolis force and the inner mass vibrates along y-axis in sensing mode. This vibration of inner mass along y-axis is relative

to the angular rate. Equations (2) and (3) below express the motion of the MEMS gyroscope.

$$(m_1 + m_2)\ddot{x} + c_1\dot{x} + k_1 x - 2m_2\Omega\dot{y} = F\cos\omega t \quad (2)$$

$$m_2\ddot{y} + c_2\dot{y} + k_2 y - 2m_2\Omega\dot{x} = 0 \quad (3)$$

In equation (2), the excitation force along x-axis is $F\cos\omega t$ [14]. From the equations (2) and (3), we can see that when the angular rate is zero, the vibration of inner mass is not proportional to the outer mass. If the gyroscope rotates with a non-zero angular rate**,** the vibration of the outer mass influences the vibration of inner mass. We can deduce the angular rate by measuring the vibration amplitude of the inner mass and utilizing the relationship between it and the angular rate.

2.2 Environmental sensing

Our environment changes continuously at varying pace. Long-term monitoring of the various parameters of the environment allows us to understand how the entire system works, predict future happenings and gives important support to effective engineering [15]. With this information, we are capable to build smarter systems. The changes in the environment are not usually rapid and dramatic so the sampling frequency does not need to be high which helps designing low-powered monitoring systems.

Heat is a physical quantity and one form of energy that is measured in energy units of joules [3]. We cannot measure quantity of heat in the object but we can measure the changes of the quantity of heat when temperature or the physical state of the object changes. In other words, temperature is a measure of the quantity of heat for an object whose physical state remains unchanged.

One common way to measure temperature is to use a thermocouple as the sensing element [3]. Two differing metals have always a contact potential between them. This potential changes accordingly to the temperature. This works only if there is two junctions in a circuit with the junctions at different temperatures. Unfortunately, the output from one thermocouple is small being roughly few millivolts for a 10 degrees temperature difference, which makes sensing small temperature changes difficult. However, connecting several thermocouples in series forming a thermopile structure increases the output linearly [16]. This increases the output and the sensitivity of the system allowing more accurate temperature measurements.

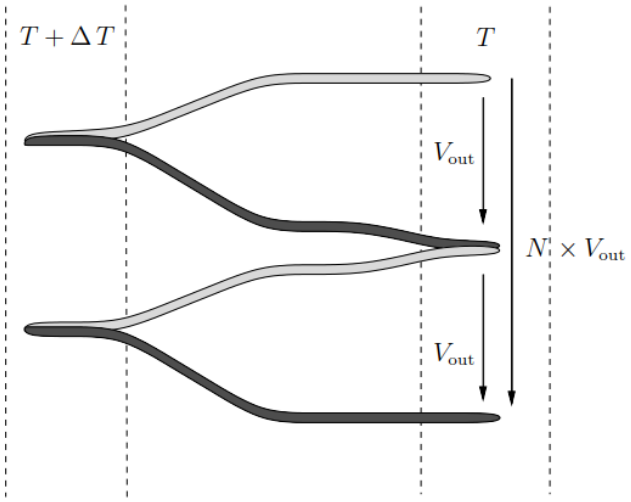

Figure 5. *Schematic drawing of a two-thermocouple thermopile [16].*

Figure 5 illustrates the basic structure of a two-thermocouple thermopile. Each thermocouple consists of two different material [16]. In the thermopile structure, the low terminal of each thermocouple connects to the high terminal of the other thermocouple. Each material has their own Seebeck coefficient α_a that is the immediate rate of change of potential V_a with respect to the temperature at a given temperature T_0. The equation (4) below describes how the Seebeck coefficient is calculated.

$$\alpha_a = \frac{dV_a}{dT}\Big|_{T_0} \tag{4}$$

Connecting more than two thermocouples in series increases the output of the thermopile structure. The equation (5) below describes how the output is depended of the number of thermocouples N.

$$V = N(\alpha_a - \alpha_b)\Delta T \tag{5}$$

Complex interactions of physical factors affect also the output voltage of a thermopile [16]. In addition to sensing temperature differences thermopiles can sense radiation with some modifications. This is the most common application for thermopiles. The equation (6) below expresses the thermal behavior of these systems.

$$\frac{\Delta T}{\Phi} = \frac{1}{G}\frac{1}{\sqrt{1+\omega^2\tau_{th}^2}} \tag{6}$$

In equation (6), the thermal time constant τ_{th} describes the detector response time to modulated radiation [16]. The equation describes how the thermal behavior of a detector structure depends on the thermal conductivity G due to a modulated radiation flux Φ at radial frequency ω.

Major of the MEMS pressure sensors utilize thin membrane to measure pressure differences [4]. The pressure difference deflects the thin membrane that induces displacement that then converts to an electrical signal. MEMS pressure sensors exploit either piezoresistive or capacitive sensing in this electrical conversion.

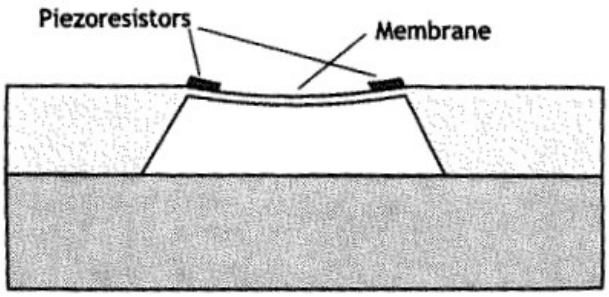

Figure 6. *The principle of piezoresistive pressure sensor [4].*

Figure 6 presents the basic structure of pressure sensors using piezoresistive sensing. The white area in the center of the sensor operates as the reference pressure that usually is in vacuum or in the normal pressure of 101.3 kPa [4, 17]. If the air pressure is greater than the reference pressure, the membrane bends downwards causing stress to the membrane. This stress causes a change in resistance of the piezoresistors. The maximum stress takes place near the edge of the membrane. This is the most beneficial place to install the piezoresistors. Pressure sensors using piezoresistive sensing have advantages like simple measuring circuitry, quite linear response and built-in shielded structure of piezoresistors. However, they consume lots of power, depend greatly on temperature and suffer noise due to piezoresistors. Because of these disadvantages and the demand for small battery powered devices, capacitive pressure sensors are constantly gaining market share.

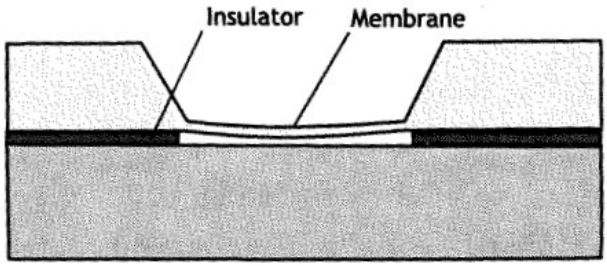

Figure 7. *The principle of capacitive pressure sensor [4].*

Figure 7 illustrates the basic structure of pressure sensors using capacitive sensing. Like in the piezoresistive sensing, the white area in the center operates as the reference pressure and the external air pressure bends the thin membrane. The displacement of the membrane causes a change in the capacitance between the membrane and a fixed electrode [4, 17]. The air pressure is than calculated by measuring this capacitance. The main advantage of pressure sensors using capacitive sensing are the low power consumption and excellent

noise performance. The disadvantages are the nonlinear capacitance behavior, the complicated measuring circuitry and the vulnerability to parasitic capacitances.

$$A = \frac{v_{out}}{p} = \frac{C_0 v_{in}}{C_f d_0} w_a \tag{7}$$

The equation (7) above describes the complete sensor transfer function of the capacitive pressure sensor. The complete sensor transfer function is the outcome of the output voltage depending on the difference between the external and the reference pressure [4]. In the equation, C_0 represents the capacitance when there is no bending in the membrane, v_{in} is the sense voltage, C_f represents the feedback capacitance of the measuring system, d_0 is the electrode gap and w_a is the average displacement of the membrane.

The term humidity describes the existence of moisture in a gas [3]. Usually this moisture is water and gas is air. The absolute humidity illustrates the mass of water per unit mass of gas. In many cases, the relative humidity, which is the absolute humidity divided by the value of saturated humidity at that temperature, is more useful than the absolute humidity. This is because the humidity depends heavily on the current temperature. Nowadays, the most popular commercial humidity sensors are relative humidity sensors using either resistive are capacitive sensing [18, 19]. Both of these sensing methods focus on measuring impedance differences due to changes in humidity.

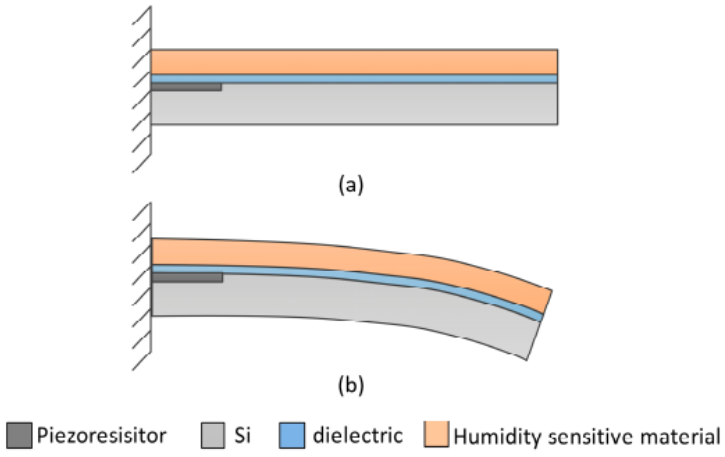

Figure 8. *The principle of piezoresistive humidity sensor and the status of the sensor in (a) low humidity and (b) high humidity [18].*

Figure 8 presents the basic structure and the operation of a humidity sensor using piezoresistive sensing. High humidity induces moisture to the humidity sensitive material causing it to expand [18]. This expansions causes stress to the structure. The piezoresistor converts this stress into an electrical signal. The main advantages of piezoelectric humidity sensors are ease of fabrication, simple measurement circuitry, high linearity and long-term stability. The biggest drawback are long recovery time, low stability limit and temperature drift. Adding a specific circuit can though compensate the temperature drift.

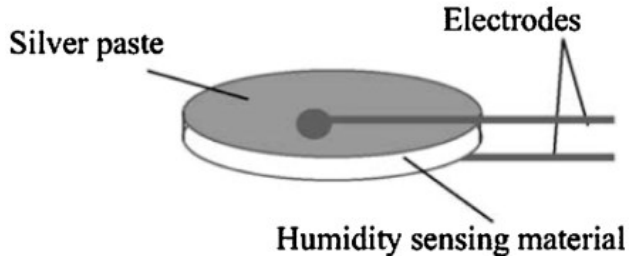

Figure 9. *The principle of capacitive humidity sensor [19].*

Figure 9 illustrates the elementary structure of a humidity sensor using capacitive sensing. In this structure, humidity sensing material is between two electrode plates [18, 19]. High humidity induces moisture to the humidity sensing material changing its dielectric constant. The change of the dielectric constant causes a capacitive change that is measured. The needed measuring circuitry can be complex but is the only disadvantage of capacitive humidity sensing. The advantages compared to piezoelectric humidity sensing are lower power consumption, wider temperature range, simpler manufacturing, higher reliability and lower cost. Due to these advantages, capacitive humidity sensors dominate market share compared to resistive humidity sensors.

2.3 Magnetic sensing

There are many commercial and industrial applications for magnetometers. Reason for this is that they make possible safe, non-invasive, non-destructive means of detection and additionally give a more durable, reliable and maintenance-free technology compared to other technologies [20]. Most of the sensing methods of magnetic fields utilize the intimate connection between magnetic and electric phenomena [21].

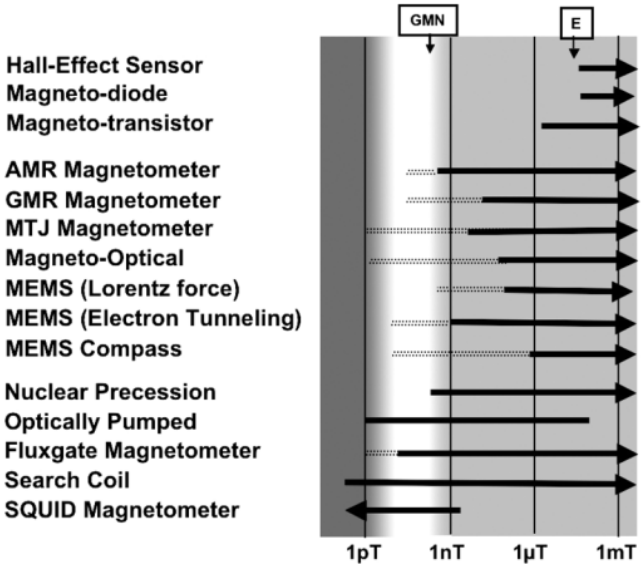

Figure 10. *Estimate of sensitivity of different magnetic sensors. E represents the strength of the Earth's magnetic field and GMN is Earth's geomagnetic noise [21].*

There are several methods to sense magnetic fields. Figure 10 lists the most popular and common magnetic sensing technologies and represents the estimation of sensitivity of each of them. Earth's magnetic field is large in magnitude that needs attention in sensor design [21]. Magnetic sensors usually compensate this with either having large dynamic range or using a coil to decrease the field at the position of the sensor. Anisotropic Magneto-Resistance (AMR) and Hall Effect sensors are the most used sensors among the industrial markets [22]. When comparing these two, AMR sensors have higher sensitivity, smaller dynamic range, better thermal stability and lower dc offset while Hall Effect sensors have a wider bandwidth. Other advantage of Hall Effect sensors is that hysteresis and saturation phenomena do not limit their performance as they do with AMR sensors. One major disadvantage of AMR sensors is that they have great power consumption to achieve acceptable field resolution due to having a low sensitivity to magnetic field [23].

Among consumer markets, MEMS magnetic sensors are gaining market share [22]. MEMS magnetic sensors generally utilize Lorentz force transduction for magnetic sensing. Like Hall Effect sensors, they are immune to hysteresis and saturation phenomena [23]. They do not also need any specialized magnetic materials. Other advantages are small power consumption, high resolution and easy integration with other MEMS sensors.

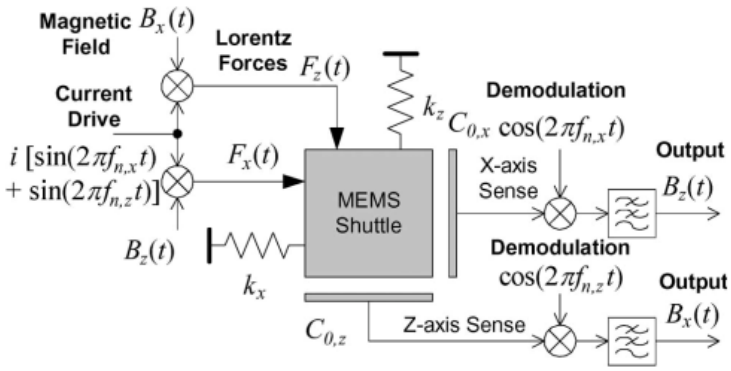

Figure 11. *Block diagram of MEMS magnetic sensor using Lorentz-force sensing [23].*

MEMS magnetic sensors using Lorentz-force sensing usually utilize either piezoresistive or capacitive sensing in measurements [22]. Figure 11 represents the basic block diagram of the operation of the MEMS magnetic sensor using Lorentz-force and capacitive sensing. The operation is similar to a three-axis MEMS accelerometer [23]. An external magnetic field causes Lorentz force on the MEMS structure inducing motion to the shuttle. Sense capacitors around the shuttle detect this motion transforming it to an electrical output. Adding an ac current drive to the structure generates Lorentz force that centers at the sensors mechanical natural frequency. This amplifies the resulting motion, allows frequency-selective detection and reduces sensitivity to acceleration and cross-axis magnetic fields.

$$F_L = Li \times B \tag{8}$$

The equation (8) above illustrates the relationship between magnetic field B and Lorentz force F_L in a wire with length L carrying a current i. The Lorentz force is normal to the direction of the current flow, which means that a wire aligned with y-axis experiences forces in x- and z-axis. Usually MEMS magnetic sensors use current-carrying flexures instead of straight wires [23]. In this case, effective length L_e replaces wire length L.

2.4 Positioning

Many variables affect the landing position of the elevator. Even if we could get the engine to lower the cable the absolute same amount each time, the elevator car would still land on different level each time due to number of other purely mechanical reasons [24]. The main reasons for this are the elevator steel rope and the suspensions system of the elevator car. The length of the steel rope varies depending on the forces pulling it according to the Hooke's law. The higher the elevator shaft is the greater the variation of the length will be. The weight of the passengers affects directly on the suspension level of the elevator car. These occurrences combined can create unsafe floor level differences, which could lead to accidents among passengers walking through the door. However, using a steel rope with lower expansion rate or removing the suspension system is not reasonable due to reason that they remove most of the vibration during the movement of the elevator car.

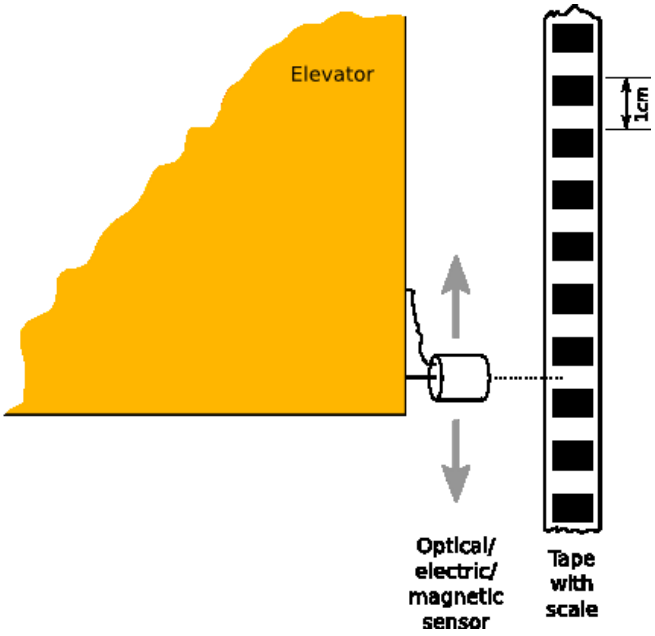

Figure 12. *The principle of absolute floor position measurement using an encoder [25].*

Currently, there are few methods to measure the position of the elevator car in the elevator shaft. All these methods utilize encoders in measurements [24]. The most accurate position systems use the same measuring principle as in Figure 12. Tape with scale or in other words code tape is installed vertically to the entire length of the elevator shaft and a sensor using optical, electric or magnetic sensing is installed to the elevator car. Because the expansion of the steel rope and the suspension system cannot affect the code tape, the

sensor will always read the absolute position of the elevator car in the shaft. There are number of different manufactures who produce position systems utilizing this measuring method [26-28]. These products can measure the position of the elevator car that is travelling 20 m/s in up to 1500 m high elevator shafts with accuracy of fraction of millimeter. The problem is that they are very expensive to install and maintain especially afterwards to older elevators.

We could instead of vertically installed encoders use relative rotary encoders like odometers. Odometers measure the rotation of the wheel [24, 29]. This wheel can be the main shaft of the motor or a traction wheel or other governor wheel. Odometer transforms this measured angular distance into linear travelled distance according to the wheel size. In addition to travelled distance, odometers can also measure the speed. The measured data can be as accurate as in previously mentioned position systems but are much cheaper. However, because the odometer measures the distance from a wheel, the measurements are vulnerable to errors from many sources, such as the steel rope slipping, temperature and both wearing out and ageing of wheels and other components.

For the sensor node, we need a position measurement system that does not require expensive parts and complex installation. A cheap solution is to utilize motion and environmental sensors and a method called dead reckoning. Figure 13 illustrates the principle of the dead reckoning. Dead reckoning measures the change in position [29]. First dead reckoning needs to have a known start point. Then it measures the travelled distance with installed sensors and adds it to the previous position obtaining the estimation of the current position. This repeats when moving to the following position. In other words, the dead reckoning is the sum of a series of relative position measurements.

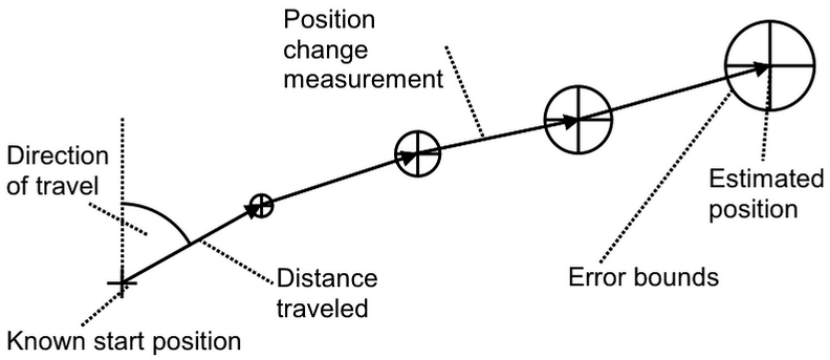

Figure 13. *The principle of the dead reckoning [29].*

A complete three-dimensional dead reckoning navigation system forms an inertial navigation system (INS) [29]. Usually INS utilizes only three orthogonally placed accelerometers and gyroscopes. In addition to INS, the dead reckoning can exploit other sensors like a magnetometer and a barometric altimeter to get measurements that are more accurate. Especially altimeters using pressure sensing improve navigation accuracy in height estimation [30]. The accuracy of the data from altimeters is high enough to determine the

correct floor of a user in a multi-storey building. Using sensor fusion methods in integration of inertial sensors with environmental sensors, suits well for motion tracking applications.

No matter how accurate sensors the positioning system utilizes, all sensors suffer from tiny inaccuracies and noises [3, 4, 29]. Each measured change of position will then have an error. Because the dead reckoning position solution is a sum of series of relatively measured positions, the error in the position will also be a sum of series of errors. Thus, the error in the position will grow with time. The figure 13 demonstrates this growing error. In addition to these errors, the usage of the altimeter brings a few problems. The resolution of altimeters is usually around 1-10 Pa that corresponds to 0.1-1 m at sea level [29, 30]. The pressure sensor can also lag if the height increases or decreases rapidly. However, unpredictable atmospheric conditions, like opening and closing of doors and air condition systems, are the main reason for errors. The INS suits well for tracking short distances but for longer distances INS needs to utilize some kind of position fixing techniques, sensor fusion methods or some other method to compensate the errors [31]. Skog et al. state that the traveling elevator car could be tracked for up to 43 seconds with an error of less than 1.5 meters in 99.9 % of the time with just accelerometers [6].

A better solution could be to use a ranging system to measure the position of the elevator car in the shaft. In ranging, the system sends a radio-frequency, ultrasonic or optical signal onto an object and processes the reflected signal to determine the distance [32]. For elevator shaft conditions, a suitable ranging method would be either a light detection and ranging (LIDAR) or a sound navigation and ranging (SONAR) system.

LIDAR utilizes optical distance measuring methods. It typically utilizes laser pulses generated by semiconductor laser diodes [33]. Semiconductor laser diodes have minimum width and high peak power that are only limited by the capability of a laser drive and safety regulations. Laser itself is an acronym of Light Amplification by Stimulated Emission of Radiation [34].

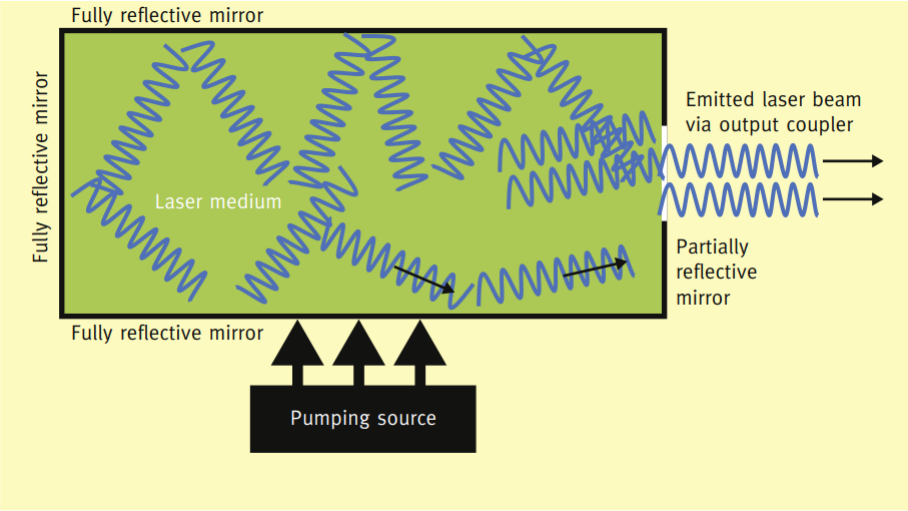

Figure 14. *The structural components of a laser [34].*

Figure 14 presents the basic structural components of a laser. The three main components of a laser are laser medium, excitation system and optical resonator. The laser medium can be solid, liquid or a gas and consists of atoms with electrons in discrete orbital shells. The pumping source operates as the excitation system and supplies energy to the lasing medium, which causes electrons to move between different energy levels and emit energy. The arrangement of mirrors operates as the optical resonator, amplifies the emission and allows it to exit from one end. The output is the actual laser beam that is electromagnetic radiation with monochromatic, collimated and coherent nature.

SONAR systems utilize ultrasound, which is a high frequency acoustic wave above 20 kHz [35]. Normal human ear cannot hear this but many animals can, like bats, dogs and dolphins. The producing of ultrasonic soundwave starts with an oscillator. The oscillator creates a high-frequency electrical signal. A transmitter transforms this electrical signal into mechanical vibrations of the same frequency. These mechanical vibrations generate sound waves of the same frequency aimed towards the target. The target reflects the sound waves causing echo, which causes an electrical signal in the receiver.

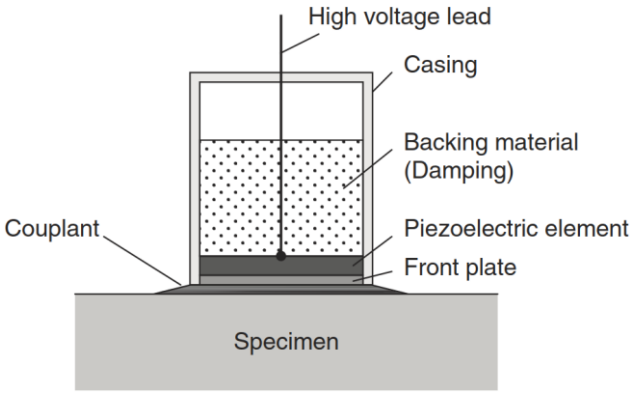

Figure 15. *The basic construction of a piezoelectric ultrasonic transducer [36].*

There are many ways to create sound waves but the most used transducers high-frequency purposes are utilize piezoelectric materials [35, 36]. Exposure of an electric field causes piezoelectric crystals to change dimensions. The piezoelectric crystals will change the dimensions with the same frequency of an alternating voltage. This works also the other way round. Exposure of an ultrasonic wave induces vibration with the same frequency to the piezoelectric crystals generating a voltage. Thus, a piezoelectric transducer can operate as both a transmitter and a receiver. Figure 15 represents the basic construction of a piezoelectric transducer. The front plate and the casing provide protection from external and environmental influences. The backing material reduces unwanted ultrasonic waves reflected inside the casing. The high voltage lead transports the electric signal between the operating system and the piezoelectric element.

Nowadays, the most used methods in both LIDAR and SONAR applications are time-of-flight (TOF) and triangulation [32, 35]. With triangulation, we could capture the shape and the color of the surface of the object accurately. This requires careful design considerations. Especially the projection system is the most critical element in achieving high-resolution results. Usually only 3-D digitizing applications use triangulation method. For a basic distance measurement, triangulation is quite exaggerated.

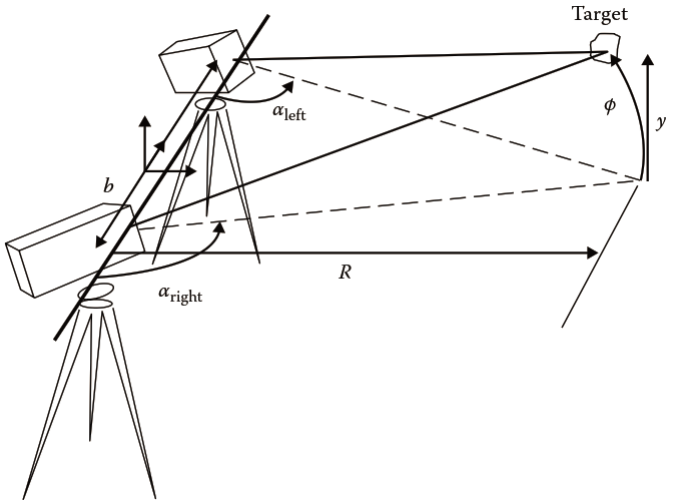

Figure 16. *The principle of triangulation [35].*

Figure 16 illustrates the basic triangulation geometry. The idea of triangulation bases on the information of the length of one side of a triangle and two of its angles [35]. With this information, we can calculate the other side of the triangle with equation

$$R = \frac{b \sin \alpha_{left} \sin \alpha_{right}}{\sin(\alpha_{left} - \alpha_{right})}. \tag{9}$$

In Figure 16, the baseline *b* between the projector and the detector represents the known side of the triangle. The lines from the projector and the detector to the target called lines of detection form the other sides of the triangle. Pointing angles α_{left} and α_{right} form between the detection line and the baseline. The disadvantage of triangulation is that it

is only accurate in short distances. Due to geometry considerations, the error sources will increase with the square of distance.

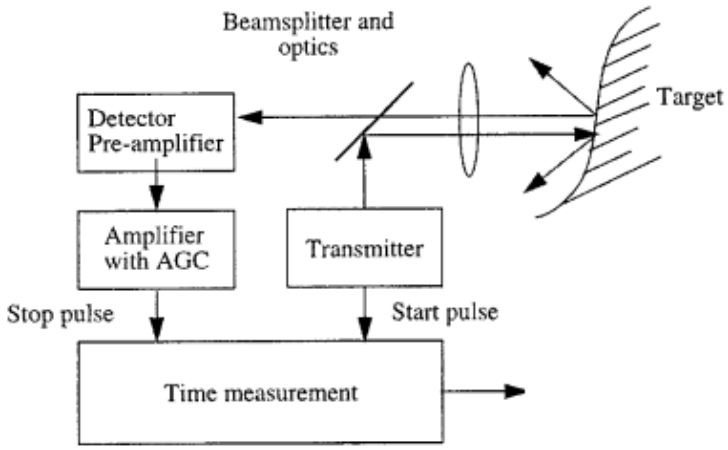

Figure 17. *The principle of the TOF ranging [32].*

Figure 17 represents the block diagram of the TOF ranging technique. The transmitter sends a pulse of energy towards the target where the pulse reflects and travels back to the detector [32, 33]. The detector amplifies the received signal and transmits it to the amplifier with an automatic gain control (AGC). The amplifier transmits the automatically amplified signal to the time measurement block. The TOF technique measures the time it takes for this round trip. The emitted pulse triggers the time measurement on and the reflected pulse stops it. This time interval is directly proportional to the distance to the target. The distance is then the outcome of the following equation

$$d = \frac{ct}{2}. \tag{10}$$

The measured time *t* represents the whole distance travelled by the pulse with a known velocity *c.* This distance is twice the distance between the measurement system and the target. Thus, reducing the measured time by half gives the actual range *d* to the target. The benefit of TOF ranging is the direct nature of sensing as both the transmitted and received signals follow mainly the same path between the measurement system and the target.

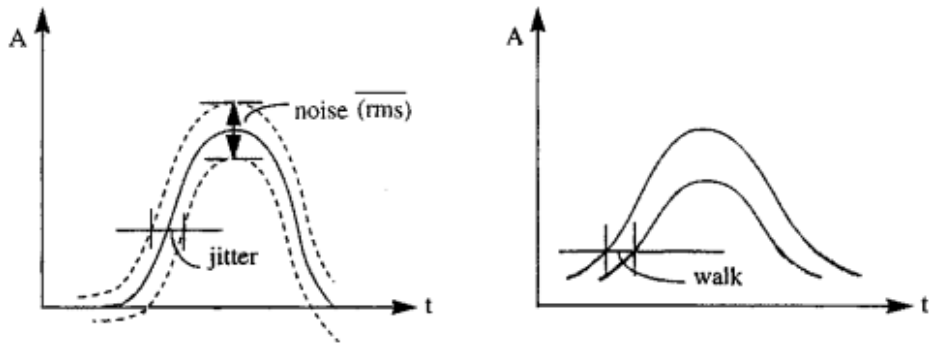

Figure 18. *Timing jitter and walk in TOF time measurements [32].*

The accuracy of the TOF ranging depends on the time interval measurement [32, 33]. There are though many sources for inaccuracies, like jitter, noise and walk. Figure 18 illustrates the effect of these errors. Jitter is the error in timing and determines essentially the precision of the measurement. Electronics and background radiation inflict noise that mainly affects the amplitude of the measured signal. Walk is timing error in the time-pickoff circuit that pulse amplitude and shape variations create. A careful design of each component of the measurement system and utilizing various compensation techniques can reduce these errors significantly but may in addition increase expenses [32]. Also using a technique called averaging improves greatly the distance measurement. The improvement is proportional to the square root of the number of results averaged.

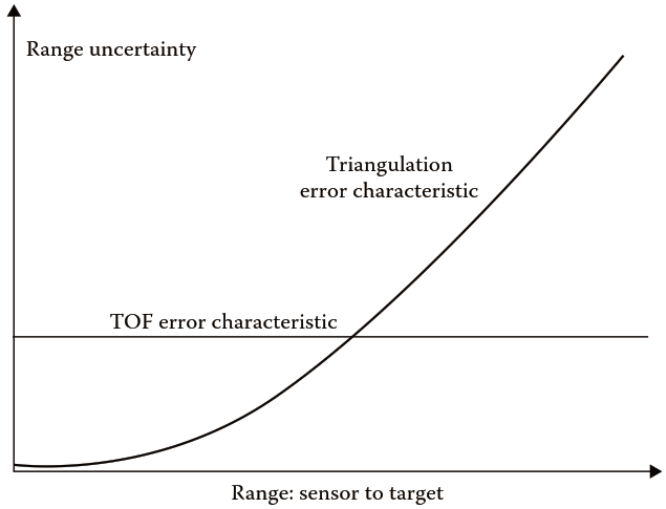

Figure 19. *The error comparison between triangulation and TOF [35].*

Figure 19 demonstrates the error behavior in TOF and triangulation in relation to range. The shortest measurable time interval is the dominant error source in TOF systems. Even though that error can be large, it is also constant and independent of distance. However, in triangulation the error depends on distance and increases with the square of distance. Thus, triangulation provides more accurate results than TOF only in short distances. In other cases, TOF provides more accurate results than triangulation.

Although LINAR and SONAR systems utilize similar ranging methods, they need to take different kinds of considerations in their applications due to distinct physical natures between light and sound. The biggest difference is the velocity in the air. If the TOF ranging system uses laser as the pulse, the velocity of the pulse will be the speed of light that is roughly 30 cm/ns [32]. To achieve the accuracy of 1 mm, the used time interval measurement should be 6.7 ps. If the same system use sound as the pulse, the velocity will be in normal temperature and pressure (NTP) 343 m/s [35]. To achieve the same accuracy, the used time interval measurement should be only 5.8 µs. Even though SONAR systems achieve the high accuracy more easily than LIDAR systems, the speed of sound is much more complicated parameter than the speed of light. The speed of light is a physical constant but the speed of sound depends on air pressure, air temperature and the chemical composition of air [35, 36]. In great distance measurements, large temperature gradients in the environment can cause erroneously calculated distances. Measuring the environmental values and compensating the measurements with them can compensate the calculations up to some level [36].

2.5 Commercial elevator monitoring systems

Some big elevator manufacturers have already responded to the opportunities provided by highly topical IoT. Many state of the art maintenance services utilize intelligent monitoring systems that exploit smart sensor systems, cloud services and IoT. There are also a few other companies, which are not elevator manufacturers, providing this kind of maintenance services.

Otis is the world's largest manufacturer of people-moving products and provides a remote monitoring product called REM (Remote Elevator Monitoring) [37]. REM has been active maintenance strategy for over two decades. With REM, expert technicians are able to monitor elevators 24 hours a day 365 days a year. REM collects data from elevator sensors and is able to proactively detect and report factors that may interrupt elevator operation. It provides both wireless and telephone line connectivity for monitoring purposes. Otis offers REM only for its own elevators.

Schindler is a Swiss manufacturer providing people-moving products, maintenance and modernization services and has a service program called Schindler Ahead [38]. Schindler states this to be the world's first fully digital closed loop maintenance, monitoring, and information system. In this program, technicians install a device called the Cube to the elevator. The cube collects data and transmits it wirelessly to the cloud. In addition to this, it runs apps, streams multimedia content and handles emergency data. Ahead keeps the cube up to date by providing over-the-air secure software updates. The cloud connects equipment, customers and passengers with Schindler's customer service network and technicians and keeps everyone informed at all times. Just like REM, Ahead predictively identifies, analyzes and resolves possible service issues before they occur all the time with advanced analytics and machine learning.

Kone is a Finnish elevator and escalator manufacturer providing also solutions for maintenance and modernization and provides service program called 24/7 Connected Services [39]. In 24/7 Connected Services program, a monitoring equipment is installed to an elevator. This equipment gathers constantly information from the elevator's parameters, usage statistics and faults using the latest technology. Then an advanced analysis system processes this gathered data and identifies the need for maintenance. According to how critical the need is, it alerts directly a technician or contacts technical support. The program sends clear notifications and reports about the actions performed keeping the customer aware of what is going on.

Thyssenkrupp is a German elevator company and offers an elevator maintenance program developed with Microsoft called MAX [40]. Thyssenkrupp states MAX to be the industry's first real-time, cloud-based predictive maintenance solution. MAX utilizes Microsoft Azure as a cloud platform. MAX claims to offer ultra-fast and low-cost computing and data storage when compared to rival systems. Like REM and Ahead, MAX collects data from elevators, sends it to the cloud. The cloud analyzes the data for patterns, computes equipment's operation and the remaining lifetime of components and delivers diagnostics to technicians in real time.

Ace Lifts is an English company providing lift control systems to various lift companies. They also provide an elevator remote monitoring systems called the i-COM [41]. The i-COM is compatible with any elevator. It connects to the encoder and control panel. The user interface receives collected data via the CAN Bus system. The i-COM is open-protocol meaning that it can be added to any company's equipment and not be tied with using Ace Lifts. The i-COM only provides tools for monitoring but not any advanced data analytics or machine learning diagnostics for predictive maintenance.

Dexdyne is an English enterprise offering web-based remote monitoring for all equipment [42]. Their remote management system consists of a remote communication terminal and a secure cloud server. The system suits for retrofitting to existing lift installations irrespective of manufacturer. The terminal of the system connects directly to the monitored equipment and communicates via a default Modbus protocol. The communication between the terminal and the cloud utilizes either wireless or wired connection. The cloud offers simple and intuitive monitoring solutions and interactive charts. The terminal can send SMS alerts to engineers when elevator needs service or attention. Pre-emptive maintenance is possible but requires trend monitoring.

3. DEVELOPED SENSOR SYSTEM

The main task was to develop a sensor system for elevator monitoring that can capture all the crucial occurrences, like vibration and movement. In addition to this, the other task is to implement a positioning system that can determine the position of the elevator car in the shaft. The developed prototype should also withstand the conditions of elevator shaft and be easy to install and operate.

3.1 Instrumentation

The idea in building the prototype was to use available ready-made commercial components. Doing this speeds up the building of the prototype and gives more time to implement other important areas to the prototype. The control board was the only thing that was not commercial product but manufactured instead.

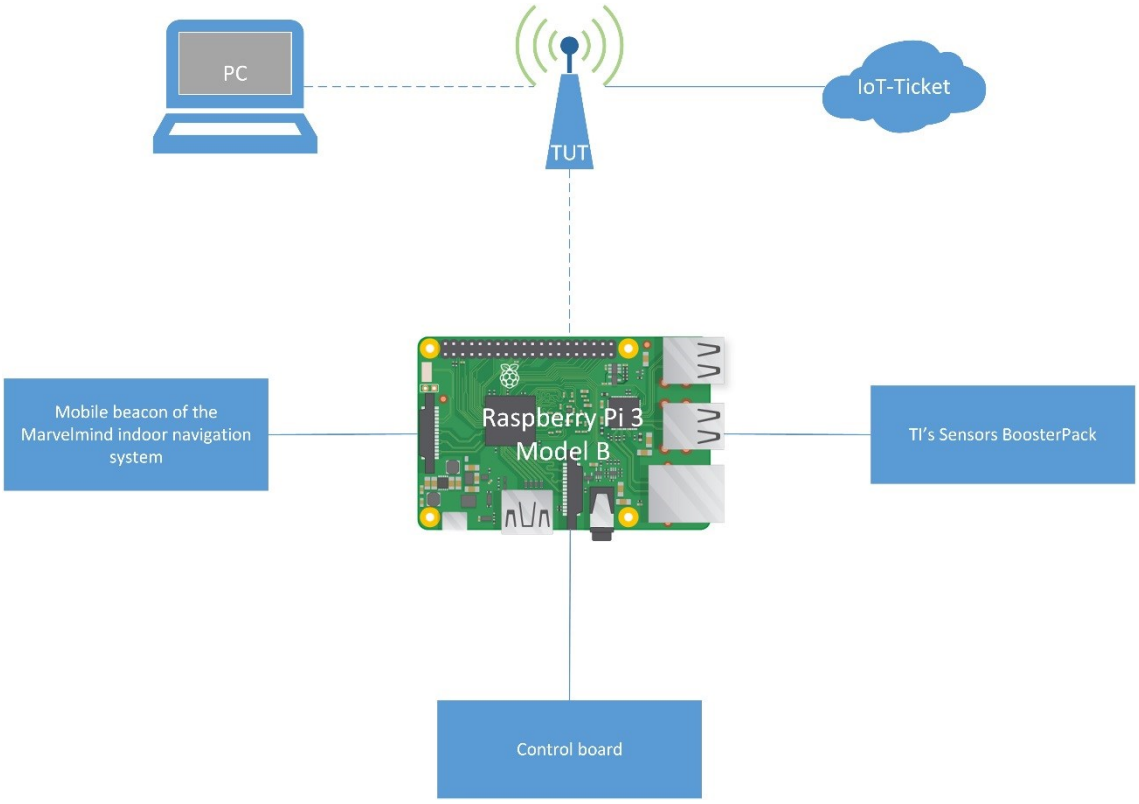

Figure 20. *The block structure of the developed sensor system.*

Figure 20 presents the block structure of the developed sensor system. The base of the prototype is Raspberry Pi 3 model B. All the motion and environmental sensors are in one Texas Instruments' (TI) plug-in module, which connects to Raspberry via inter-integrated circuit (I2C). Marvelmind's indoor navigation system provides the positioning and connects via universal serial bus (USB) to Raspberry. The control board connects to the

Raspberry's general purpose input/output-pins (GPIO). The prototype connects wirelessly to the wireless local area network (WLAN) called TUT provided by Tampere University of Technology (TUT). This enables the use of remote access with personal computer (PC) using Secure Shell (SSH) and storing data to a cloud server. It utilizes IoT-Ticket as the cloud server. IoT-Ticket is a product of Wapice. The system gets power from an external power bank. Figure 21 presents the final prototype of the developed sensor system.

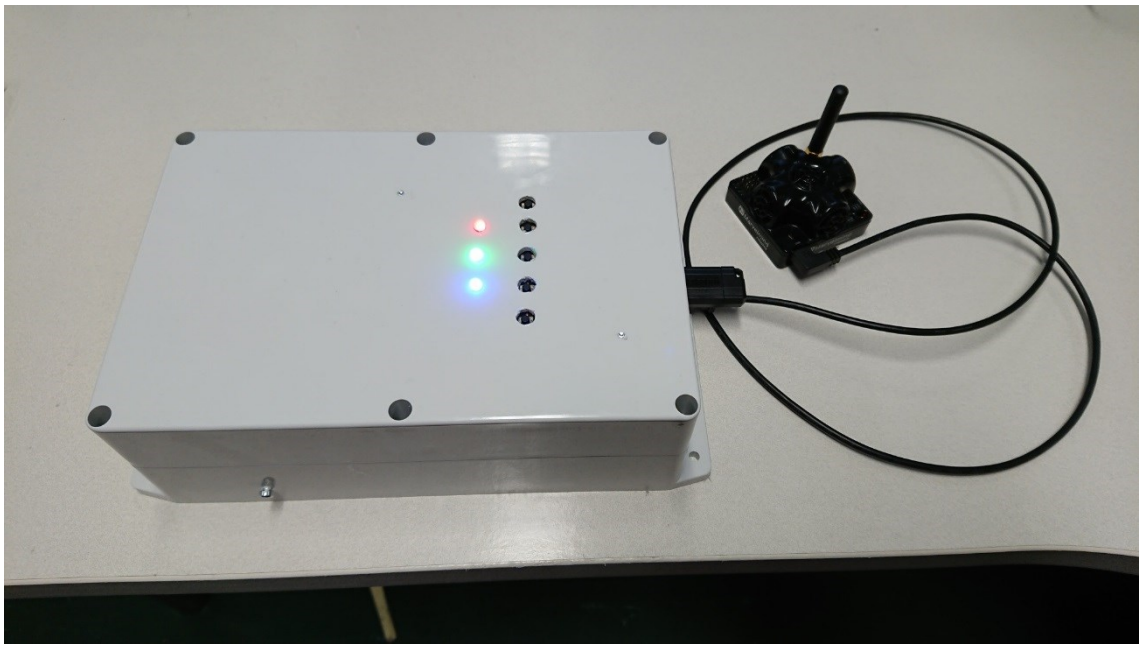

Figure 21. *The final prototype of the developed sensor system.*

3.1.1 Raspberry Pi 3 model B

Eben Upton came up with the idea of the first Raspberry Pi when he noticed that the general state of young students' experience of computer science decreased all the time [43]. The idea was to create a simple and cheap tool for educational purposes. Basically Raspberry Pi is a low-priced computer with the size of a credit card. Eventually Upton teamed up with his colleagues and set up Raspberry Pi Foundation. In February 2012, they released the first commercial Raspberry Pi. The Raspberry Pi Foundation sold over a million Raspberry Pis in the first year of business and became the fastest-growing computer company in the world ever.

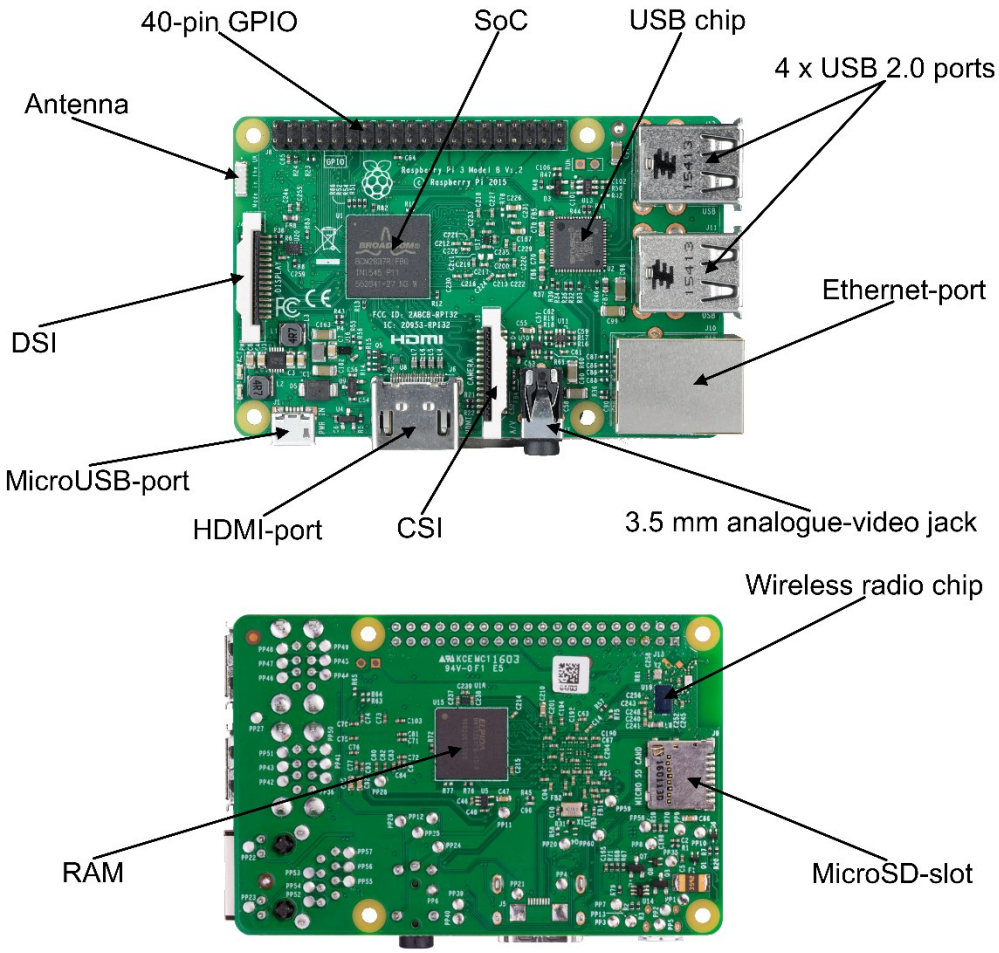

Figure 22. *Raspberry Pi 3 Model B adapted from [44, 45].*

The developed prototype utilizes Raspberry Pi 3 that is currently the latest generation of Raspberry Pis. Figure 22 represents the used Raspberry Pi 3. Table 1 lists the specifications of Raspberry Pi 3. Raspberry Pi 3 utilizes especially built BCM2837 system-on-chip (SoC) manufactured by Broadcom [46]. The chip includes both the central processing unit (CPU) and the graphics processing unit (GPU) and connects to a 1 GB random access memory (RAM) module. The other Broadcom chip, BCM43438, installed on the Raspberry provides all the wireless connections and connects to the antenna chip. The chip has also FM radio receiver but that feature is disconnected. Raspberry Pi 3 has three different ports for video output: high definition multimedia interface (HDMI), 3.5 mm analogue-video jack and display serial interface (DSI). DSI-port is mainly used only with the official Raspberry touch screen. The SMSC LAN9514 chip handles the Ethernet connectivity and four USB 2.0 channels of the Raspberry. External components connect to the Raspberry via either USB or GPIO. MicroSD-card acts as the main storage where the operating system, programs, files and other data are installed. The Raspberry Pi 3 utilizes external power supply that connects via a microUSB-port.

Table 1. *The specifications of Raspberry Pi 3 Model B [46].*

SoC	Broadcom BCM2837
CPU	4 × ARM Cortex-A53, 1.2 GHz
GPU	Broadcom VideoCore IV
RAM	1 GB LPDDR2, 900 MHz
Networking	10/100 Ethernet 2.4 GHz 802.11n wireless
Bluetooth	Bluetooth 4.1 Classic Bluetooth Low Eenergy
Storage	MicroSD
GPIO	40-pin header
Ports	HDMI 3.5 mm analogue-video jack 4 × USB 2.0 Ethernet Camera Serial Interface (CSI) Display Serial Interface (DSI)

The Raspberry in the developed sensor system uses Raspbian as the operating system. Raspbian is an unofficial port of Debian, which is a free operating system and utilizes Linux kernel [47]. It includes basic set of programs and utilities for programming and general use like Python, Java and Mathematica [48]. Raspbian is also the official supported operating system of the Raspberry Pi Foundation.

3.1.2 TI Sensors BoosterPack

The Sensors BoosterPack is a plug-in module primarily meant for TI's Launchpad development kit developers [49]. The module includes gyroscope, accelerometer, magnetometer, pressure, ambient temperature, humidity, ambient light, and infrared temperature sensors. All the sensors in the module communicate via the same I2C-interface. The module has 20-pin female and male header on both sides. In addition to power and I2C-connection, the various inbuilt interrupt-signals from sensors are also mapped to these headers.

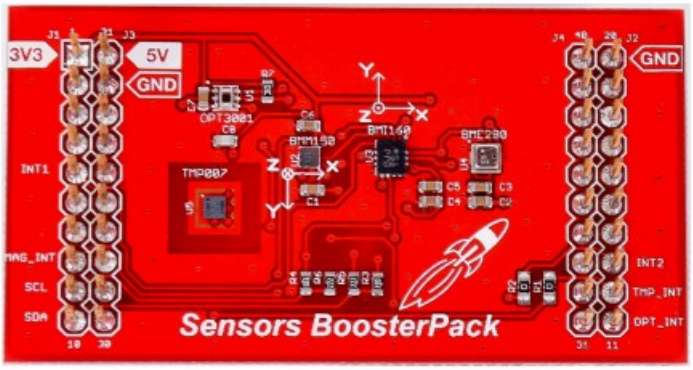

Figure 23. *Sensors BoosterPack plug-in module [49].*

Figure 23 represents the module and the five different MEMS sensors installed. The available sensors are OPT3001, TMP007, BMM150, BMI160 and BME280 [49]. OPT3001 is an ambient light sensor manufactured by TI and TMP007 is a contactless infrared thermopile temperature sensor manufactured also by TI. The developed sensor system does not exploit these sensors. The reason for this is that the intensity of light does not give any valuable knowledge about the elevator condition and a temperature sensor is already included in BME280. Therefore, the developed sensor system utilizes only BMM150, BMI160 and BME280 in measurements and elevator condition monitoring.

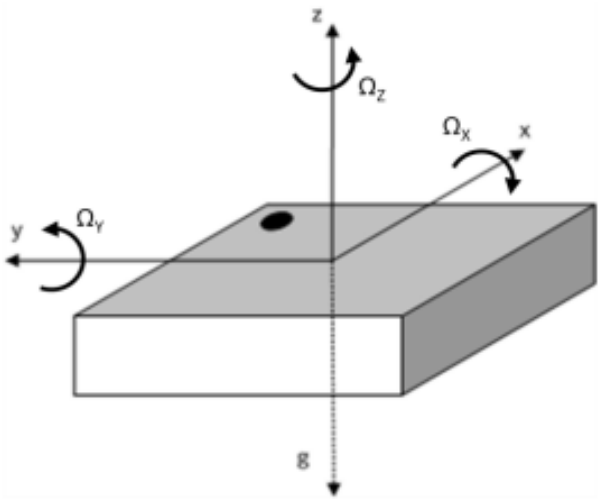

Figure 24. *The sensing axes orientation of BMI160 sensor [50].*

BMI160 is an inertial measurement unit that includes a 3-axis low-g accelerometer and a 3-axis low power gyroscope [50]. Figure 24 shows the orientation of these sensing axes. If the sensor at rest stationary and z-axis points upwards, all channel readings should be zero except the output of the acceleration channel z that should be +1 g. The user can set the acceleration range to be ±2g, ±4g, ±8g or ±16g and the gyroscope range to be 125 °/s, 250 °/s, 500 °/s, 1000 °/s or 2000 °/s. The resolution in both sensors is 16 bits. BMI160 includes an interrupt engine that provides motion-based gesture recognition, like any- or no motion detection, orientation detection and free-fall detection. The maximum output data rate of the accelerometer is 1600 Hz as with the gyroscope it is 3200 Hz.

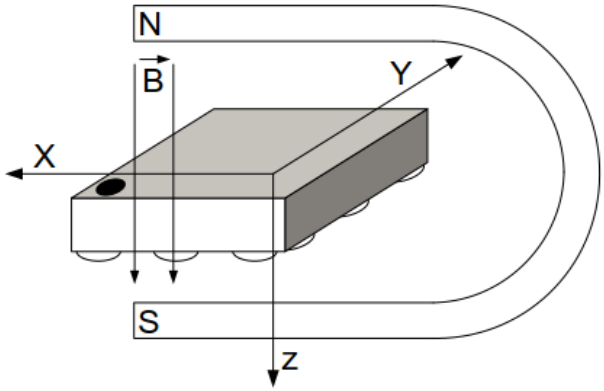

Figure 25. *The sensing axes orientation of BMM150 sensor [51].*

BMM150 is a geomagnetic sensor that measures magnetic field in three perpendicular axes [51]. Figure 25 presents the orientation of these three sensing axes. If for example the x-axis points towards the Earth's north pole, the measured value will be negative due to the Earth's north pole is a magnetic south pole, the measured field is negative, Maximum measurable magnetic field ranges are in x- and y-axis ±1300 µT and in z-axis ±2500 µT. The resolutions of these measurements are 0.3 µT. BMM150 features also an interrupt engine like BMI160. In the module, BMM150 connects as slave to secondary I2C interface of BMI160 [49]. In this configuration, the settings and the data acquisition of BMM150 are in the control of BMI160 [50].

BME280 is an environmental sensor featuring pressure, humidity and temperature sensing [52]. The measurable pressure range is from 300 hPa to 1100 hPa with a resolution of 0.18 Pa. BME280 measures with full 0-100 % relative humidity (RH) range when the temperature is between 0 °C and 60 °C. Outside of these thresholds, the RH range is limited. The resolution of the humidity sensor is 0.008 %RH. The measurable temperature range is from -40 °C to 85 °C with a resolution of 0.01 °C. The accuracy of each sensor improves with usage of oversampling. BME280 offers the measurements to be oversampled 1, 2, 4, 8 or 16 times. While oversampling improves accuracy, it also slows down the measurement time and decreases the sampling frequency.

3.1.3 Marvelmind indoor navigation system

Marvelmind indoor navigation system is a commercial relative positioning system manufactured by American Marvelmind Robotics [53]. The system consists of beacons and a modem represented in Figure 26. User configures a beacon to be either stationary or mobile. The function of stationary beacons is to form a map where the system can track the mobile beacon. The system calculates the distances between beacons automatically based on TOF and trilateration. The system is functional for both 3D and 2D tracking.

Figure 26. *Marvelmind indoor navigation system consisting of five beacons and a modem [53].*

Each beacon has five ultrasonic sensors installed [53]. All these sensors face different directions and have approximately 90° of ultrasonic coverage. This means that one beacon has 360° of ultrasonic coverage in xy-plane and 270° in xz- and yz-plane. The used frequency of ultrasonic signals is 31 kHz. The maximum distance between two beacons can be up to 50 meters in perfect lab conditions but in other environment, the maximum reachable distance is about 30 meters. Each beacon knows only its own position in the map. The supported interfaces for obtaining the location data from a beacon are universal asynchronous receiver transmitter (UART), serial peripheral interface (SPI), virtual UART and standards of The National Marine Electronics Association (NMEA). The user can use virtual UART-interface via USB and other interfaces via the external 4x4 pinout installed on every beacon.

The modem controls the whole positioning system [53]. It communicates with beacons via a proprietary radio protocol. The system utilizes industrial, scientific and medical (ISM) radio band, which is 433 MHz in this assembly. The modem sets up the system, monitors it and interacts with the dashboard. It knows every beacons position in the map. The supported interfaces for obtaining location data of beacons are UART, SPI and virtual UART. The user can use virtual UART-interface via USB and other interfaces via the external 2x8 pinout installed on the modem.

The user configures and monitors the system with the dashboard via computer [53]. Even though the system automatically creates the map, the user can with the dashboard modify or create even more complex map. With the dashboard, the user can also see and modify the settings of beacons and the modem. The dashboard saves all the settings to the modem. Therefore, once all the settings are done, the user can use the system without the dashboard.

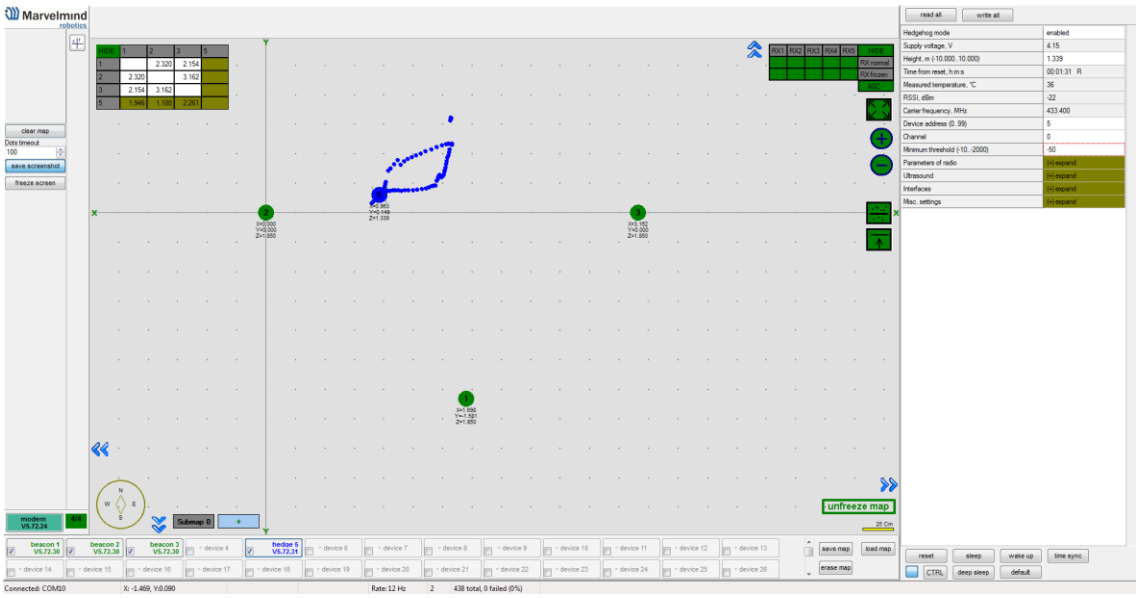

Figure 27. *The view of the dashboard used to set up and monitor the Marvelmind indoor navigation system.*

Figure 27 presents the view of the dashboard on computer. In the center of the view is the map. Green circle icons with numbers present stationary beacons. The blue circle icon with number presents the mobile beacon in active mode. In sleep mode, it is transparent. Blue small dots are the previous locations of the mobile beacon. The table in the top left corner presents the distances between beacons. The user can do all the settings of the beacons, the modem and the map in the menu on the right.

The sampling frequency of the mobile beacon depends on many variables [53]. The range of the sampling frequency is from 0.5 to 45 Hz, which the user can set manually. The maximum sampling frequency depends on the distance between beacons, the number of mobile beacons and the radio interface profile. Short distances between beacons increases the sampling frequency. Using more than one mobile beacon decreases the sampling frequency. For example, if the used sampling frequency is 25 Hz and the number of mobile beacons 3, the actual sampling frequency is 25/3 Hz. Increasing the radio interface profile increases the sampling frequency but also decreases the coverage are of the radio.

Beacons are powered with either a 1000 mAh battery or an external power supply via microUSB [53]. The battery life depends on the used sampling frequency. Table 2 presents expected working times of beacons with the 1000 mAh battery. Increasing the sampling frequency decreases the expected working time of a beacon. The modem is powered only with an external power supply via microUSB.

Table 2. *The expected working time of a beacon with the 1000 mAh battery [53].*

Sampling frequency (Hz)	Hours	Days	½-days
1	1352	56.3	112.7
4	376	15.7	31.3
8	192	8.0	16.0
16	97	4.0	8.1

The most crucial factor for the positioning to be accurate is the placing of the stationary beacons [53]. Stationary beacons should provide ultrasonic coverage for the whole area where the mobile beacon will be moving. Obstacles and other objects in the map area cause shadows to the ultrasonic coverage inflicting inaccuracy to the positioning. Installing a beacon on long sound-conducting objects can cause disturbance to ultrasonic signals. Installing beacon on relatively soft material, that does not conduct sound, prevents this phenomenon.

The ultrasonic coverage area is limited due to the maximum distance between beacons being around 30 m usually. Marvelmind offers a solution to increasing the ultrasonic coverage area with a feature called submap [53]. A submap is part of the map covering just part the map and including only subset of used beacons. Only the beacons in one submap need to be within 30 m distance of each other. One submap needs to have at least two beacons. Submaps can have one or two common beacons with other submaps that helps the dashboard to position the submap correctly to the map. Creating more submaps to the map increases the trackable distance of the mobile beacon. For example, creating three submaps to the map increases the maximum trackable distance up to 90 m.

Marvelmind navigation system promises that it can measure the distances between beacons with relative accuracy of ±2 cm when the user has adjusted the system parameters correctly with environmental values [53]. The main cause for inaccuracies in positioning is erroneous ultrasound speed that mainly depends on temperature, pressure and moisture like mentioned in chapter 2.5. Marvelmind states that temperature is the main factor and the distance error between the absolute and the measured distance is 0.17 %/°C. This means that for example with distance of 30 m and temperature error of 5 °C the distance error is $0.17\ \%/°C \cdot 5\ °C \cdot 30\ m \approx 0.255\ m$. Because the system utilizes trilateration on calculating distances, small errors in measurements cause bigger errors in positioning.

3.1.4 Control system

The user can control the prototype with either a computer via SSH or the manufactured control board. Using SSH, the user can access the command line of the raspberry remotely with a SSH client, like PuTTY. For the remote access using SSH, the user needs to have the computer and the prototype in the same network and know the Internet Protocol (IP) address of the sensor system.

The prototype connects wirelessly to the wireless network called TUT. This makes remote access to the sensor system possible all around the campus of TUT. However, the reception of wireless networks is weak in some elevators disabling the usage of SSH. Thus, the prototype needs a separate control board.

Figure 31, Figure 32 and Figure 33 in appendix A present the designed control board to operate the prototype. The control board consists of 5 switches and 3 light-emitting diodes (LED). Each LED is capable of glowing in red, blue or green. Four switches have pull-down resistors and capacitors installed to decrease debouncing. The fifth switch connects directly to the reset port of the Raspberry.

3.2 Software

The main task of the prototype is to collect and store data from the used sensors. Other tasks are that the sensor system is easily controllable and can store data into the cloud server. The software is stored and executed in the Raspberry. It is written completely in Python using the development environment and tools provided by Raspbian OS.

3.2.1 Structure

Figure 28 illustrates the software of the developed sensor system as a block structure. In the beginning, the system boots up and initializes the sensors. After the initialization, the system is ready to measure. In this state, the user has four different options: start the measurement, offset calibration, cloud saving or shutdown the system. The offset calibration is recommended to perform first. This compensates the offset for BMI160 sensor eliminating possible errors due to the sensor system is not exactly horizontal. After the calibration, the software comes back to the previous state. The user can then start the measurement. The software launches three individual processes each measuring and storing data from own sensors. When the user triggers the measurement off, the software terminates the processes and copies the measured data files to a memory stick if available. After this, the software returns back to the original state. After first measurement, the cloud saving is possible. The process first checks, if the internet connection is established, and then sends the last measured files to the cloud server. After this, the software returns to previous state. If the software cannot establish internet connection or IoT-Ticket is not accessible, the process informs this with LEDs and returns to the previous state. The fourth option is to shut down the system. During the shutdown, the software clears the registers and resets the parameters of the sensors.

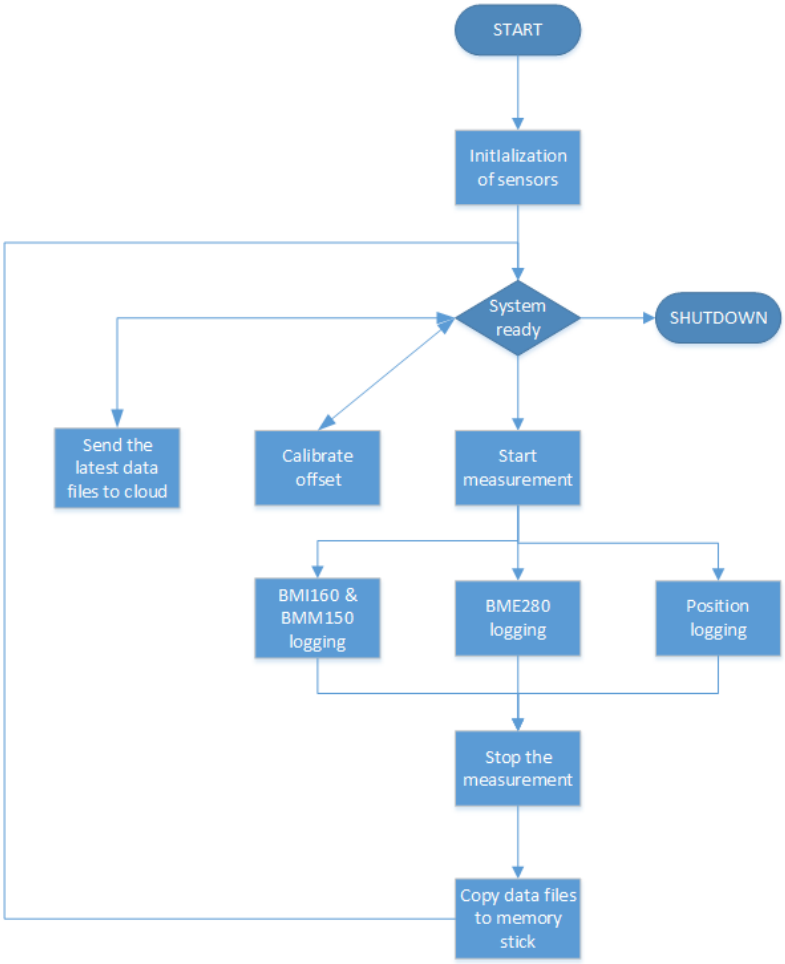

Figure 28. *The block structure of the software of the developed sensor system.*

The software utilizes a few readymade Python libraries. It gets the measured position data from the Marvelmind indoor navigation system using the library provided by Marvelmind Robotics [54]. Saving data to the cloud server of IoT-Ticket utilizes the library provided by IoT-Ticket [55]. The library to read and collect data from BME280 sensor is adapted from the library made by Matt Hawkins [56]. The library to read and collect data from BMI160 and BMM150 sensors are self-made.

During the initialization of the sensors in the beginning, the software sets the used parameters to the sensors. The sampling frequency of accelerometer, gyroscope and magnetometer is 400 Hz. The range of accelerometer is ±2 g and the range of gyroscope is ±125 °/s. The initialization sets temperature, humidity and pressure sensors oversample 4 times, which turns out as a typical sampling frequency of 37.7 Hz according to the formula of the measurement rate given in the datasheet [52].

The software collects the data and logs it to output files. The measured and stored variables are date, time, Unix timestamp, acceleration in 3-axis, rate of turn in 3-axis, magnetism in 3-axis, resistance of the hall sensor plate, temperature, relative humidity of air, air pressure and position in 3-axis. The software utilizes multithreading and collects the

data with three independently working process. The first process collects the data from BMI160 and BMM150 sensors, the second process collects the data from BME280 sensor and the third process collects the data from Marvelmind positioning system. Each process logs the data to own output file in comma-separated values (CSV) format.

The software utilizes the fast offset compensation function that is an inbuilt function in BMI160 sensor. It compensates the output values of accelerometer and gyroscope. This is useful due to that there is always a bit of offset in the horizontal positioning of the prototype when installed to the elevator car.

3.2.2 Data processing

The software stores the data files in CSV-format to the internal memory that is the SD-card in Raspberry Pi. When the logging is paused, the software automatically copies the data files to the memory stick via USB. This enables the user to obtain quickly and easily the data files and to transfer them to own computer for further research.

The software stores the data into three separate files. In the beginning, the software creates a folder for the current test day, in which the data files are stored. First file stores the data from BMI160 and BMM150 sensors. The samples from BMI160 and BMM150 sensors are unsigned 16-bit integers. The software transforms and saves them to data files as signed decimal integers. In further research, these values must be scaled according to the defined sensor parameters. The second file contains the data from BME280 sensor. The software stores the compensated samples from BME280 sensor in real units to data files. The third file contains the data from the Marvelmind positioning system. The Marvelmind positioning system produces the positioning samples in cm-unit with accuracy of 0.1 cm with own timestamp.

The software can also copy the data files to the IoT-Ticket cloud server if necessary. The user can do this after the logging is paused and the data files copied to the memory stick. The time it takes to send the data files to the cloud depends on the size of the data files and the speed of the internet connection.

4. RESULTS

The main task of the developed sensor system is to monitor elevator systems. Some of the features of the prototype were tested in real elevator systems. The positioning tests of the Marvelmind positioning system was not done in real elevator system. Instead, the testing was done in an environment simulating an elevator shaft. Doing this made more accurate testing of the Marvelmind system possible.

4.1 Test arrangements

All the tests were performed at TUT campus area. The tests focused on the performance of the developed sensor system in obtaining the data from sensors and logging it correctly. The data logging of the sensors except positioning was tested in real elevator systems. The positioning was tested in a separate test setup.

The tests in real elevator systems were done to verify that the developed sensor system could log the data from BMI160 and BMM150 sensors with a sampling frequency of 400 Hz. In addition to this, the movements and other events of the operation of the elevator car should be visible in the measured data. During the elevator tests, the prototype was placed on the floor of the elevator car like in Figure 29 and was controlled via the control board. Controlling the prototype via SSH was not possible due to poor WLAN reception in elevators.

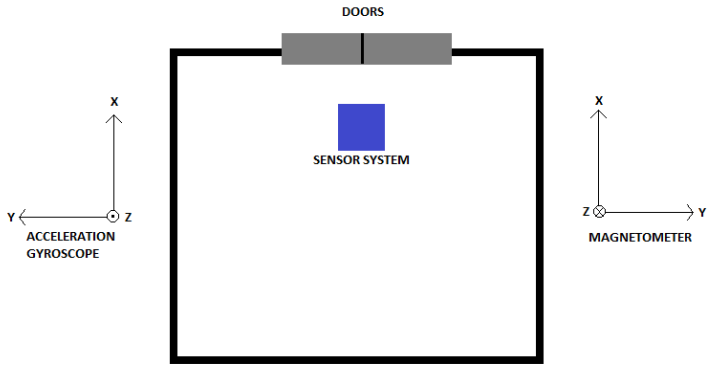

Figure 29. *From above view of the prototype on the floor of the elevator car with oriental axes.*

The tests with Marvelmind indoor navigation system were performed to verify that the developed sensor system could log the data correctly from the mobile beacon and find

out the accuracy of the repeatability in the positioning. The object was to test what is the reachable repeatable accuracy with this system. The positioning was preliminary tested in a separate test, in which we simulated the operation of the elevator car in the corridor of Konetalo at TUT. Creating a separate test setup allowed us to test the system more precisely than in a real elevator system. Two different positioning tests were performed to find out the repeatable accuracy of the Marvelmind indoor navigation system.

A separate software was coded for these positioning tests. With this software, the user could do the positioning measurements remotely with a computer via SSH. Triggering the measurements remotely eliminates the positioning errors that the user could cause by triggering the measurements via control board. Once the user triggers the measurement, the software takes 100 positioning samples provided by Marvelmind system and stores them into a file in CSV-format. The files are stored both to internal memory and to memory stick. Each separate positioning measurements are stored to an own separate file for easier handling and further research.

The typical length of the corridor of Konetalo is around 65 m. The stationary beacons were positioned around 22 m apart each other covering the whole corridor from end to end like in Figure 34 in appendix B. One beacon was installed to each end of the corridor with soft adhesive material and two other beacons were installed evenly distributed along the corridor with soft adhesive material. The map consisted of three submaps and each submap consisted of two stationary beacons. First submap consisted of beacons 1 and 2, second submaps consisted of beacons 2 and 3 and third submap consisted of beacons 3 and 4. Beacon 5 was the mobile beacon.

The setup of the first test simulated the operation of the elevator car with 10 different floors. Figure 34 in appendix B represents the layout of the first test arrangements. The idea of the floor pattern was to test out every possible area of the map. The floors were positioned the way that the test would clarify the repeatable error in each submap and between submaps. The distance between floors from floor 1 to floor 9 was 3 m that is a typical height difference between floors in an elevator shaft [57]. Floor 10 was positioned to the middle of submap 3.

Figure 30. *The first prototype installed on the trolley during the first positioning test.*

The prototype and the mobile beacon were on a trolley like in Figure 30, which simulates the elevator car and the corridor represents the elevator shaft. The mobile beacon was installed with soft adhesive material to the trolley. The trolley was first positioned accurately to the floor 1. Then the prototype was triggered to take 100 position samples. After that, the trolley was moved to the next floor, in this case to floor 2, and another 100 position samples was taken. These steps were repeated until the trolley reached floor 10. After the prototype had taken 100 position samples in floor 10, the trolley was positioned back to floor 1 and the whole procedure was repeated. The procedure was repeated five times meaning we had taken five times 100 position samples from each floor. The idea behind this test was to find out that, when we leave the floor and come back to the same floor again, how accurately the Marvelmind system gives the same positioning results.

The trolley was each time positioned accurately to the current floor with a commercial laser tape measurer. We used Bosch GLM 100 C as our laser tape measurer. Its typical measurement accuracy is ± 1.5 mm, the typical deviation influence is ± 0.05 mm/m and the typical measurement range is 0.05 – 80 m [58]. It can also be controlled remotely with smartphone via Bluetooth. The laser tape measurer was installed to one end of the corridor pointing towards the trolley like in Figure 34. The distance measurement was triggered remotely with smartphone via Bluetooth disabling the influence of position error that the user causes when operating the laser tape measurer physically.

The second positioning test was to find out how accurately the Marvelmind system works during the shift from one submap to another. The stationary beacons were installed similarly like in the first test except the beacon 4 was not installed being unnecessary. Figure 35 in appendix C presents the layout of this test setup. In this test, there was total of 11 locations. The idea of the location pattern was to test out the transaction from one submap

to another and how does measuring the position close to a stationary beacon affect the results. Location 6 was positioned to be on the same level as beacon 2. The distance between locations was 30 cm making the distance between location 1 and location 11 be 3 m. The prototype and the mobile beacon were on the trolley acting as the elevator car. The prototype used the same software for measuring as in previous test. The progress of the test was similar to the previous test. The trolley was positioned to the location 1 according to the laser tape measurer, 100 position samples were taken, moved to location 2, 100 position samples and on and on until we reach location 11 from where the trolley is positioned back to location 1. The procedure was repeated five times meaning we had taken five times 100 position samples from each location.

4.2 Measurements and interpretation of data

In appendix D, Table 3 and Table 4 represent samples of data files created by the prototype with BMI160, BMM150 and BME280 sensors. We can see that the software stores the samples from sensors correctly and the sampling frequencies are what we expected. When calculated with Matlab, the typical sampling frequencies are for inertial measurements 398.6 Hz and for environmental measurements 39.4 Hz.

The data files from the tests were researched and plotted with Matlab. Figures in appendix E presents the data of two different elevator cars in a test where one person travelled from floor 1 to floor 3 and back. The other elevator is an older elevator whereas the other elevator is practically new elevator being just few years old. The test began when the person was in the elevator car with doors open. After that, the doors closed and the elevator car moved two floors up. Once the elevator car reached the upper floor, the doors opened, the elevator waited few seconds, the doors closed and the elevator car moved back to the original floor. The test ended when the doors opened.

From Figure 36, we can clearly identify that the elevators have different acceleration profiles in z-axis. In older elevator, the acceleration profile is quite rectangular-shaped and the deceleration profile has clearly two pulses meaning that the elevator decelerates first into slow speed, positions to the correct floor and then stops. In newer elevator, the acceleration profile is much more smoothened and rounded almost resembling sinusoidal wave. We can also see that in both elevators the movement of the doors cause some vibrations to the elevator car in all 3-axis. In addition to this, we clearly see all the vibrations during the elevator car operations in all 3-axis. The older elevator has clearly more vibrations during the operation than the newer elevator.

Figure 37 present the data captured from the gyroscope. The data shows that both elevators rotate around the y-axis during the operation. From x- and z-axis, we cannot clearly identify anything without filtering the data. Elevator cars normally slide against guide rails, which reduces most of the rotation. The elevator car clearly does not rotate much

during the normal operation. Because of this, vandalism, jumping or deviations in guide rails would be visible in the data.

Figure 38 illustrate the data captured from the magnetometer. Because the x-axis points towards the doors of the elevator car, passing doors of floors are clearly visible in the data with both elevators. The passing doors inflict peaks to the data in x-axis. The operation inflicts similar peaks also to the y-axis even though they are harder to see in the data from the old elevator. In the new elevator, the opening and closing the doors of the elevator car is also visible in the x-axis. The magnetometer uses the resistance of the hall sensor only for the compensation. It does not give any major information for the measurements, which is why it is not researched further.

Figure 39 present the data captured from BME280 sensor. In both elevators, the altitude of the elevator car is well visible. When the elevator car moves up, the air pressure decreases and vice versa. The relative humidity and the temperature does not show anything special as expected during the normal and healthy operation of the elevator car.

Appendix F presents the results from the first positioning test. Figure 40 presents 100 positioning samples obtained from each test on each floor. The position samples seem to concentrate around the spot on each test instead of spreading evenly throughout the ±2 cm relative accuracy scale that Marvelmind promises. Figure 41 illustrates the normal distribution from the same results and the average from each test beneath each plot. In some cases, the separate normal distributions are concentrated quite near each other but in some cases, they have big gaps between each other. Table 5 presents the averages of these results. The table uses the averages from the first test as the reference measurement. Then it compares the other tests to the reference measurement and calculates the error between them. If the error is within ±1 cm range, it is marked with green. If the error is outside ±2 cm range, it is marked with red. The bottom and the rightmost rows present the averages of the absolute values of errors per test and floor. The value in the right bottom corner presents the total average of relative error. In most of the cases, the repeatable accuracy reaches the accuracy of ±1 cm and in some cases even better accuracy. In floor 5 and 10, the repeatable accuracy is larger than the promised accuracy of the Marvelmind system. The average of the total repeatable relative accuracy is 1.006 cm while the maximum relative error is 2.687 cm.

Appendix G presents the results from the second positioning test. Figure 42, Figure 43 and Figure 44 present 100 positioning samples obtained from each test on each location. Figure 45 shows the normal distribution from the same results and the average from each test beneath each plot. The positioning samples spread much more than in the previous test. This affects heavily to the normal distribution figures in some cases. Table 6 presents the averages of these results similarly like in first position measurement. The results are quite inaccurate from location 3 to location 8. In most cases, the repeatable accuracy is

well out of the promised accuracy of the Marvelmind system. On four locations, the repeatable relative accuracy is often within ±1 cm range. The average of the total repeatable relative accuracy is 6.437 cm while the maximum relative error is 18.793 cm. In addition to being repeatable inaccurate around a stationary beacon, the system also miscalculates the distances between locations from location 2 to location 9 demonstrated in Table 7. Table 7 presents the reference measurements of the Bosch laser tape measurer and the average results from test 1. The table lists the exact distances between floors next to each other and the total distance back to location 1. On lower rows, it lists the same measurements from test 1 and the calculated errors. The results show that the positioning is not accurate if the mobile beacon is within a distance of ±1 m from a stationary beacon in this map layout.

4.3 Defining sensor system parameters

Like the measurements show, every elevator is unique and behaves differently. This makes defining universal parameters for the sensors more complicated. The measurements show that the used parameters were suitable and did not max out in any situation.

The developed sensor system measures inertial movements with sampling frequency of 400 Hz. With high sampling frequency, the prototype can measure physical phenomenon that otherwise could be left unnoticed. It would need more research to find out if the used sampling frequency is high enough or unnecessarily high. Higher sampling frequency inflicts more noise to the measurements [50]. Careful filtering could remove this noise but then careless filtering could remove some vital phenomenon from the measurements.

The prototype used the smallest possible measurement range with accelerometer and gyroscope. The reason for this was to maximize the resolution of the measurements. The measurements prove that the smallest measurement range is well enough to capture the normal operation of the elevator system. It is safe to assume that if any of the inertial measurement values would max out during the elevator operation, there would be something very wrong with the elevator system.

The sampling frequency of the Marvelmind indoor navigation system is highly depended on the positioning and the number of stationary beacons. The greater the distance between the stationary beacons, the lower is the sampling frequency. Increasing the number of stationary beacons also lowers the sampling frequency. During the measurements, the typical sampling frequency was 8-9 Hz, which was the highest reachable sampling frequency while covering 65 m long corridor with four stationary beacons. According to the measurements from the elevator tests, the typical stationary time of the elevator car on the floor was about eight seconds. Thus, the prototype could capture 64-72 positioning samples with the typical sampling frequency, which should be enough to determine the position of the elevator car in the elevator shaft.

The strange results from the second positioning test could be avoided by positioning the stationary beacons more densely and adjusting the submaps to overlap each other. With overlapping submaps, there would be no inaccurate jumping between submaps. This would though require installing more stationary beacons more densely to the map decreasing the sampling frequency.

The prototype would be able to determine the position of the elevator car in the elevator shaft with the Marvelmind positioning system. For this, we would need to define proper parameters for triggering the measurement. In other words, we would need to determine when to trigger the position measurement on and off. BMI160 sensor has an implemented interrupt engine with no-motion detection that the prototype could utilize to detect when the elevator car is stationary. Problem comes when defining proper threshold for the no-motion. Because every elevator behaves uniquely, defining one common threshold for all elevators is complicated. For example, the doors in the old elevator cause so much vibration that the threshold should be quite high. If we would use this same threshold for the new elevator, the no-motion detection might trigger during the elevator car operation. Another example is the situation when people walk in and out of the elevator car. The weight and the walking of people cause movement to the elevator car thus it is not stationary. The other option could be to trigger the position measurement from the movement of the doors. The position measurement would trigger on when the doors open and off when the doors close. The problem with this comes again as every elevator behaves uniquely and the movement of the doors is not always visible in the data. Thus, triggering the position measurement on and off should be designed separately for every elevator.

5. CONCLUSION

This master's thesis was part of OPENS-project funded by Tekes and industrial companies. OPENS is a parallel research project of Department of Intelligent Hydraulics of TUT and Department of Information Technologies of Åbo Akademi. The task of OPENS is to develop effective methods to predict future behavior of machine systems. The development of these methods requires lot of data from different situations. The main task of this master's thesis was to develop mobile and easy to use sensor system for the use of research.

The sensor system should be capable to monitor the movement of the elevator and the environmental values of the elevator system. The sensor system should store the data locally and be capable to send the measured data to a cloud server. The other task in this Master's Thesis was to research a suitable method to determine the position of the elevator car in the elevator shaft.

The focus on designing the sensor system was to use as many commercial products as possible to save time. The base of the developed sensor system is Raspberry Pi 3 Model B. All the used sensors are in TI's plug-in module connected via I2C to the Raspberry. The sensor system utilizes Marvelmind indoor navigation system to determine the position. The mobile beacon of the Marvelmind system connects via USB to the Raspberry. The developed sensor system connects to the Internet via TUT-wireless network enabling saving data to the cloud server. The sensor system is controlled with either a PC via SSH or the control board. It measures the inertial movement of the elevator car with sampling frequency of 400 Hz and the environmental values with sampling frequency of 40 Hz. The developed sensor system stores the measured data as CSV-files.

The developed sensor system was tested in two parts. The first part focused on the performance of obtaining the data from sensors and storing it correctly in a real elevator system. The second part focused on the performance of the Marvelmind indoor navigation system. The object was to clarify the repeatable relative accuracy of the Marvelmind system. The testing was done in the simulated elevator system in the corridor of Konetalo at TUT.

In the end, the developed sensor system worked as planned. The sampling worked correctly, the requirements for the sampling frequency were reached, cloud saving was implemented to the prototype and a method to determine the position was researched. In this regard, the tasks for this Master's thesis were achieved. Most of the features of the prototype work well but there are also some things to improve.

The prototype would get results that are more accurate if instead of placing it on the floor of the elevator car it was installed tightly to the car. When the prototype is on the floor unattached, some of the vibrations and other movements of the elevator car might not transfer to the sensors and could be missed. A solution for this could be to attach the prototype with something firm and easily removable adhesive. The prototype would still be portable and would not require serious installation to the elevator car that could possible damage it.

The Marvelmind indoor navigation system is meant for 2D- and 3D-tracking, which was a little bit overkill solution for our purposes. For measuring the stopping accuracy, 1D-tracking would be enough. The Marvelmind system provides only the calculated position in the map. It uses trilateration when calculating the position. Because of the layout of the stationary beacons, some angles in the trilateration calculations are close to zero. In 2D-tracking, this causes inaccuracy to the y-value, which causes inaccuracy to the x-value. Thus, the errors in the position samples are occasionally high.

After the positioning tests, Marvelmind released a new software with a feature to stream raw distance data [59]. With this feature, the prototype could instead of the calculated position measure the raw distance between the mobile beacon and stationary beacons. This would be much more useful information than the position in 2D- or 3D-dimension. The prototype needs only measurement in one dimension to measure the stopping accuracy. The problem is still that the python library does not support this new feature. Implementing this feature would require designing a completely new software with new algorithms and filters to obtain and process the raw distance information. This goes out of the scope of this master's thesis. Implementing this feature could instead be a topic for another research.

The oversampling of temperature, humidity and pressure sensors could be increased. Increasing the oversampling would give less noisy and more accurate samples. However, increasing the oversampling decreases the sampling frequency but the sampling frequency of BME280 does not need to be as high as used. Increasing the oversampling value to the maximum 16 would lower the sampling frequency to 10.2 Hz according to the formula of the measurement rate given in the datasheet [52]. This sampling frequency could probably be still high enough to monitor environmental variables of elevator systems.

In the future, a display could be a good upgrade to the developed sensor system. The sensor system utilizes now only LEDs to inform the current state of the program and the prototype. A display would show much more information and show this more clearly then could be possible with LEDs. Today displays are also cheap components and easy to implement.

Other upgrade for the future could be to integrate automatic filtering of data directly to the software. In addition to just obtaining and storing, the software of the prototype could possible recognize some patterns or phenomenon from data, like movement of the doors or how many floors the elevator moved. This would help researching and analyzing the data files. Also, instead of sending all raw data to the cloud server, the prototype could send only the recognized events. This would reduce the amount of data send and stored to the cloud server.

REFERENCES

[1] S.T. March, G.D. Scudder, Predictive maintenance: strategic use of IT in manufacturing organizations, Information Systems Frontiers, 2017, pp. 1-15.

[2] Machine monitoring with smart sensors, Bosch, website. Available (accessed on 30.12.2017): http://www.bosch-presse.de/pressportal/de/en/machine-monitoring-with-smart-sensors-44917.html.

[3] I.R. Sinclair, Sensors and transducers, 3rd ed ed. Newnes, Oxford, 2001, 306 p.

[4] V. Kaajakari, Practical MEMS, Small Gear Publishing, Las Vegas, Nev., 2009, 465 p.

[5] R. Bogue, Towards the trillion sensors market, Sensor Review, Vol. 34, Iss. 2, 2014, pp. 137-142.

[6] I. Skog, I. Karagiannis, A.B. Bergsten, J. Harden, L. Gustafsson, P. Handel, A Smart Sensor Node for the Internet-of-Elevators-Non-Invasive Condition and Fault Monitoring, IEEE Sensors Journal, Vol. 17, Iss. 16, 2017, pp. 5198-5208.

[7] Z. Wan, S. Yi, K. Li, R. Tao, M. Gou, X. Li, S. Guo, Diagnosis of Elevator Faults with LS-SVM Based on Optimization by K-CV, Journal of Electrical and Computer Engineering, Vol. 2015, 2015, pp. 1-8.

[8] Basic Elevator Components - Part One, Electrical Knowhow, website. Available (accessed on 30.12.2017): http://www.electrical-knowhow.com/2012/04/basic-elevator-components-part-one.html..

[9] S.L. Tu, Z.Y. Wu, B. Qian, Research of the Elevator Monitoring System Based on the Internet of Things, Applied Mechanics and Materials, Vol. 423-426, Iss. Applied Materials and Technologies for Modern Manufacturing, 2013, pp. 2380-2385.

[10] P.G. Kovalchik, F.T. Duda, Speed and position sensors for mine hoists and elevators, IAS '95. Conference Record of the 1995 IEEE Industry Applications Conference Thirtieth IAS Annual Meeting, United States, pp. 2056 vol.3.

[11] H. Lei, G. Tian, H. Zhao, Y. Mao, Z. Huang, Health monitoring for coated steel belts in an elevator system, Journal of Sensors, Vol. 2012, 2012, pp. 1-5.

[12] M. Gad-el-Hak, M. Gad-el-Hak, MEMS : applications, 2nd ed ed. CRC/Taylor & Francis, Boca Raton (FL), 2006, 450 p.

[13] P. Corke, J. Lobo, J. Dias, An Introduction to Inertial and Visual Sensing, The International Journal of Robotics Research, Vol. 26, Iss. 6, 2007, pp. 519-535.

[14] Y.W. Kim, H.H. Yoo, Design of a vibrating MEMS gyroscope considering design variable uncertainties, Journal of Mechanical Science and Technology, Vol. 24, Iss. 11, 2010, pp. 2175-2180.

[15] M.F. Acevedo, Real-Time Environmental Monitoring: Sensors and Systems, 1st ed. CRC Press, Boca Raton, 2016, 388 p.

[16] A. Graf, M. Arndt, M. Sauer, G. Gerlach, Review of micromachined thermopiles for infrared detection, Measurement Science and Technology, Vol. 18, Iss. 7, 2007, pp. R75.

[17] M. Bao, Micro Mechanical Transducers, Elsevier Science, 2000, pp. 1-378.

[18] J.Q. Huang, F. Li, M. Zhao, K. Wang, A Surface Micromachined CMOS MEMS Humidity Sensor, MICROMACHINES, Vol. 6, Iss. 10, 2015, pp. 1569-1576.

[19] T.A. Blank, L.P. Eksperiandova, K.N. Belikov, Recent trends of ceramic humidity sensors development: A review, Sensors & Actuators: B.Chemical, Vol. 228, 2016, pp. 416-442.

[20] A.E. Mahdi, L. Panina, D. Mapps, Some new horizons in magnetic sensing: high-Tc SQUIDs, GMR and GMI materials, Sensors and Actuators A: Physical, Vol. 105, Iss. 3, 2003, pp. 271-285. Available: http://www.sciencedirect.com/science/article/pii/S0924424703001067.

[21] J. Lenz, S. Edelstein, Magnetic sensors and their applications, IEEE Sensors Journal, Vol. 6, Iss. 3, 2006, pp. 631-649.

[22] S. Park, M.S. Al-Ghamdi, M.E. Khater, E. Abdel-Rahman, A Tunable MEMS Magnetic Sensor, Journal of Microelectromechanical Systems, Vol. 26, Iss. 1, 2017, pp. 255-263.

[23] M. Li, V.T. Rouf, M.J. Thompson, D.A. Horsley, Three-Axis Lorentz-Force Magnetic Sensor for Electronic Compass Applications, Journal of Microelectromechanical Systems, Vol. 21, Iss. 4, 2012, pp. 1002-1010.

[24] W.K. Tou, M.I. Vai, S.U. Cheang, Elevator absolute landing position sensor using infrared interrupter and MEMS accelerometer, 2015 5th Australian Control Conference (AUCC), Engineers Australia, pp. 366-370.

[25] A. Folkesson Lab: The Elevator control system, Uppsala University, Sweden, website. Available (accessed on 15.8.2017): https://www.it.uu.se/edu/course/homepage/pins/vt12/lab.

[26] APS - Absolute Positioning System, website. Available (accessed on 9.8.2017): https://www.cedes.com/english/Products/Elevators/APS_en.htm.

[27] Position Encoding System WCS, website. Available (accessed on 9.8.2017): http://www.pepperl-fuchs.com/global/en/classid_822.htm.

[28] Elevator industry, ELGO ELECTRONIC GmbH & Co KG, website. Available (accessed on 15.8.2017): https://www.elgo.de/en/applications/elevator-industry/.

[29] P.D. Groves, Principles of GNSS, Inertial, and Multisensor Integrated Navigation Systems, 2; 2nd ed. Artech House, Norwood, 2013, pp. 1-799.

[30] A.M. Sabatini, V. Genovese, A Sensor Fusion Method for Tracking Vertical Velocity and Height Based on Inertial and Barometric Altimeter Measurements, SENSORS, Vol. 14, Iss. 8, 2014, pp. 13324-13347.

[31] J. Tuomi, Inertia-anturien hyödyntäminen kulkuneuvojen liiketilan havainnoinnissa, in: Usage of Inertial Sensors in Observing the Motions of Vehicles Tampere University of Technology, 2014, 51 p. Available: https://dspace.cc.tut.fi/dpub/handle/123456789/22214

[32] M. Amann, M.-. Amann, T. Bosch, T. Bosch, M. Lescure, M. Lescure, R. Myllylä, R. Myllylä, M. Rioux, M. Rioux, Laser ranging: A critical review of usual techniques for distance measurement, Optical Engineering, Vol. 40, Iss. 1, 2001, pp. 10-19. Available: http://dx.doi.org/10.1117/1.1330700.

[33] S. Kurtti, J. Kostamovaara, Laser Radar Receiver Channel With Timing Detector Based on Front End Unipolar-to-Bipolar Pulse Shaping, IEEE Journal of Solid-State Circuits, Vol. 44, Iss. 3, 2009, pp. 835-847.

[34] G. Thomas, R. Isaacs, Basic principles of lasers, Anaesthesia and Intensive Care Medicine, Vol. 12, Iss. 12, 2011, pp. 574-577.

[35] J.G. Webster, H. Eren, Measurement, Instrumentation, and Sensors Handbook, Second Edition: Spatial, Mechanical, Thermal, and Radiation Measurement, 2; 2nd ed. CRC Press, Baton Rouge, 2014, 1640 p.

[36] I. Ihara, Ultrasonic Sensing: Fundamentals and its Applications to Nondestructive Evaluation, in: Anonymous (ed.), Springer Berlin Heidelberg, Berlin, Heidelberg, 2008, pp. 287-305.

[37] Remote Elevator Monitoring, Otis, website. Available (accessed on 12.9.2017): http://www.otisworldwide.com/REMElevatorMonitoring.html.

[38] Schindler Ahead, Schindler, website. Available (accessed on 12.9.2017): https://www.schindler.com/us/internet/en/service-maintenance/schindler-ahead.html.

[39] Lifting Elevator & Escalator Maintenance Services into a New Era, Kone, website. Available (accessed on 30.12.2017): http://www.kone.com/en/products-and-services/solutions-for-existing-buildings/new-maintenance.aspx.

[40] MAX - Predictive maintenance solution, thyssenkrupp Elevator, website. Available (accessed on 12.9.2017): https://max.thyssenkrupp-elevator.com/en/.

[41] i-COM Lift Monitoring, ACE Lifts Ltd, website. Available (accessed on 12.9.2017): https://acelifts.com/i-com-lift-monitoring/.

[42] Remote Lift & Elevator Monitoring Solution, Dexdyne, website. Available (accessed on 12.9.2017): http://www.dexdyne.com/remote-lift-elevator-monitoring-solution.

[43] E. Upton, G. Halfacree, Raspberry Pi user guide, 3rd; Third; 3; 3rd ed. Wiley, Chichester, England, 2014, 300 p.

[44] Raspberry Pi 3, Pimoroni, website. Available (accessed on 21.11.2017): https://shop.pimoroni.com/products/raspberry-pi-3.

[45] Raspberry Pi 3 Model B, Raspberry Pi Foundation, website. Available (accessed on 4.8.2017): https://www.raspberrypi.org/products/raspberry-pi-3-model-b/.

[46] Raspberry Pi 3 is out now! Specs, benchmarks & more, The MagPi Magazine, website. Available (accessed on 22.9.2017): https://www.raspberrypi.org/magpi/raspberry-pi-3-specs-benchmarks/.

[47] Raspbian FAQ, Raspbian, website. Available (accessed on 10.10.2017): https://www.raspbian.org/RaspbianFAQ.

[48] Download Raspbian for Raspberry Pi, Raspberry Pi Foundation, website. Available (accessed on 10.10.2017): https://www.raspberrypi.org/downloads/raspbian/.

[49] BOOSTXL-SENSORS Sensors BoosterPack Plug-in Module, Texas Instruments, Mar 2017, 27 p. Available: http://www.ti.com/lit/ug/slau666a/slau666a.pdf.

[50] BMI160, Bosch, Feb 2016, 110 p. Available: https://ae-bst.resource.bosch.com/media/_tech/media/datasheets/BST-BMI160-DS000-07.pdf.

[51] BMM150, Bosch, Apr 2016, 56 p. Available: https://ae-bst.resource.bosch.com/media/_tech/media/datasheets/BST-BMM150-DS001-01.pdf.

[52] BME280, Bosch, Oct 2015, 54 p. Available: https://ae-bst.resource.bosch.com/media/_tech/media/datasheets/BST-BME280_DS001-11.pdf.

[53] Marvelmind Indoor Navigation System Operating Manual, Marvelmind Inc., Nov 2017, 50 p. Available: http://marvelmind.com/pics/marvelmind_navigation_system_manual.pdf.

[54] marvelmind.py, Marvelmind Robotics, website. Available (accessed on 30.12.2017): https://bitbucket.org/marvelmind_robotics/marvelmind.py.

[55] IoT-Ticket Python client, IoT-Ticket, website. Available (accessed on 16.11.2017): https://github.com/IoT-Ticket/IoTTicket-PythonLibrary.

[56] bme280.py, M. Hawkins, website. Available (accessed on 16.11.2017): https://bitbucket.org/MattHawkinsUK/rpispy-misc/src/cfd86a9ea9d2c71ad501503449b080df5ee42cba/python/bme280.py.

[57] Schindler 3300, Schindler, 28 p. Available: https://www.schindler.com/content/fi/internet/fi/mobility-solutions/products/elevators1/schindler3300/_jcr_content/rightPar/downloadlist_5530/downloadList/1_1372657601321.download.asset.1_1372657601321/HEL.3300.FI_L.pdf.

[58] Bosch GLM 100 C Professional, Bosch, Dec 2016, 370 p. Available: https://www.bosch-professional.com/binary/ocsmedia/optimized/full/o233323v21_160992A232_201605.pdf.

[59] Downloads, Marvelmind Robotics, website. Available (accessed on 14.12.2017): https://marvelmind.com/download/.

APPENDIX A: SCHEMATICS OF THE CONTROL BOARD

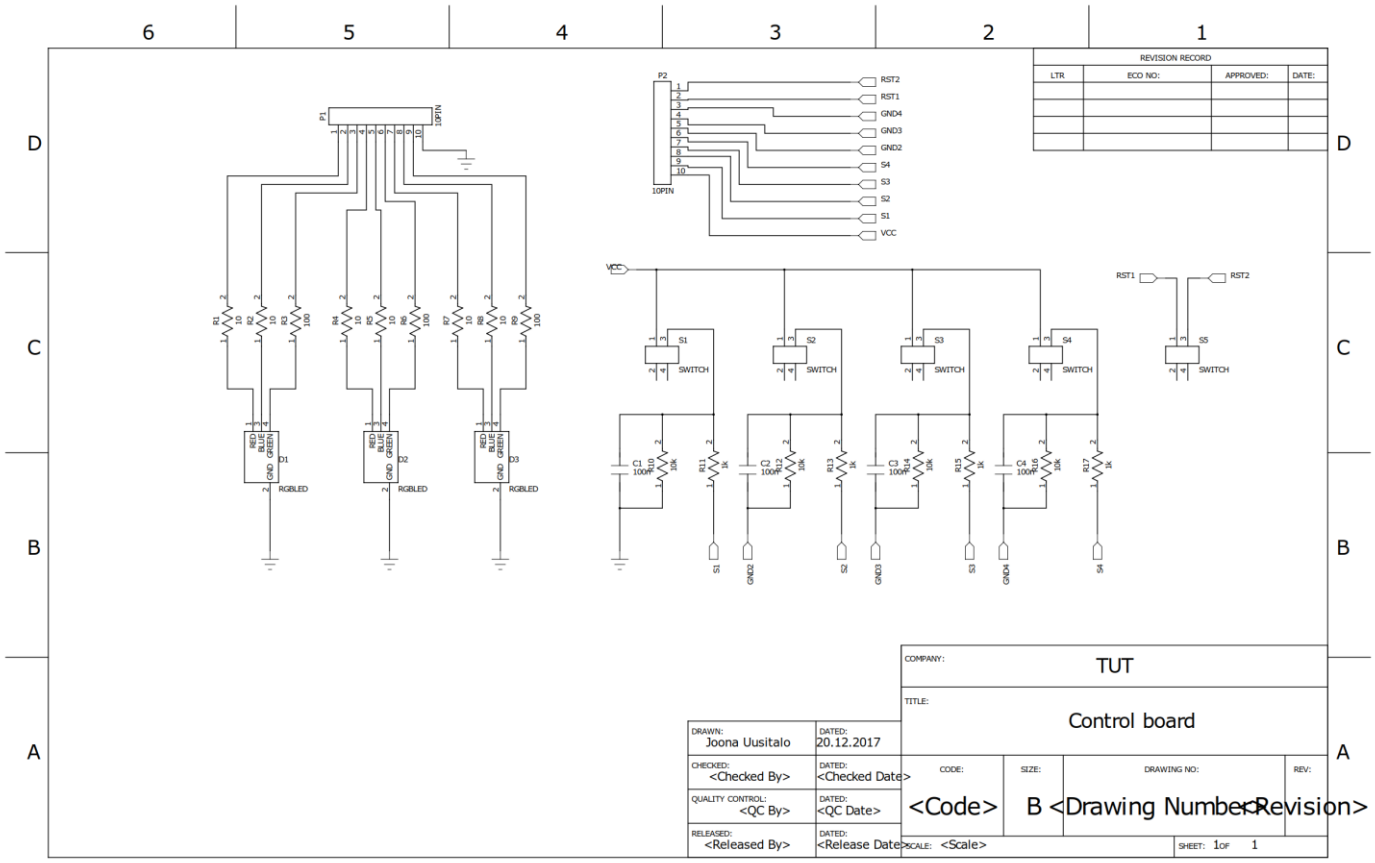

Figure 31. *The circuit diagram of the control board.*

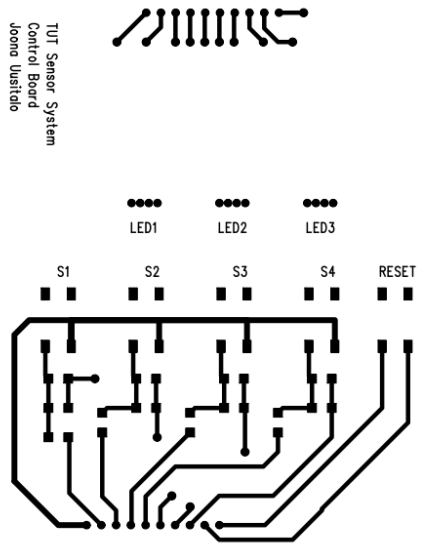

Figure 32. *The top layout of the control board.*

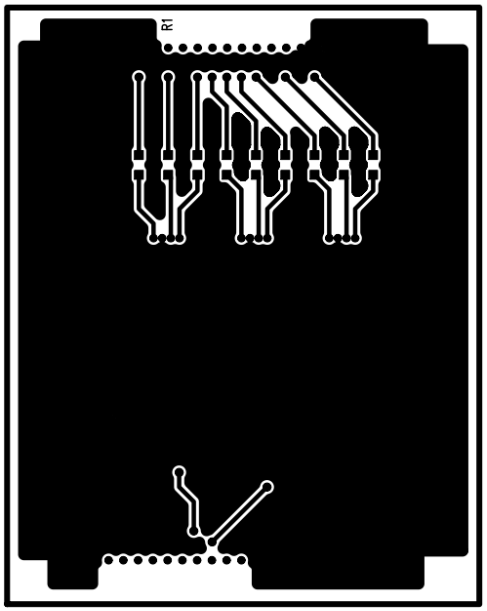

Figure 33. *The bottom layout of the control board.*

APPENDIX B: THE LAYOUT OF THE FIRST POSITIONING TEST

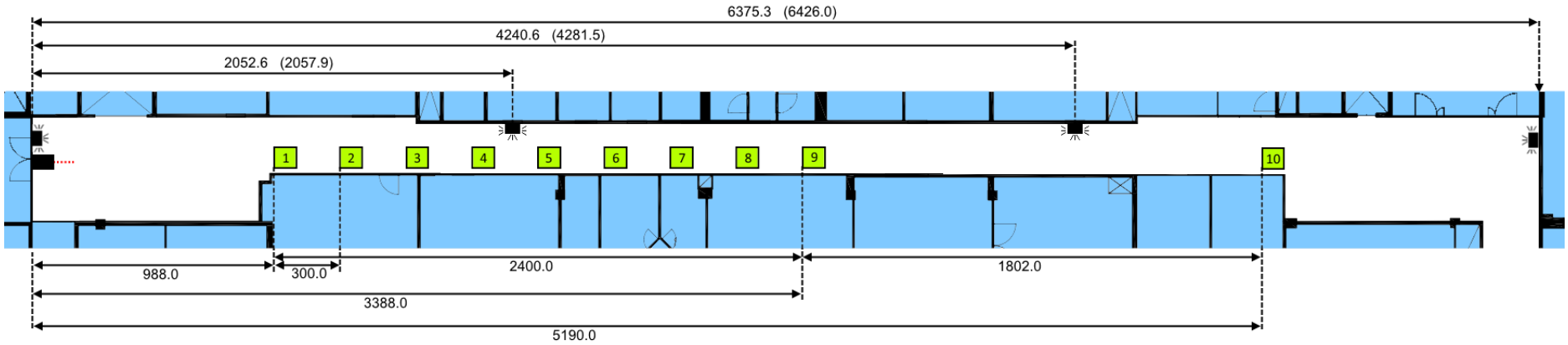

Figure 34. *The layout of the first positioning test.*

APPENDIX C: THE LAYOUT OF THE SECOND POSITIONING TEST

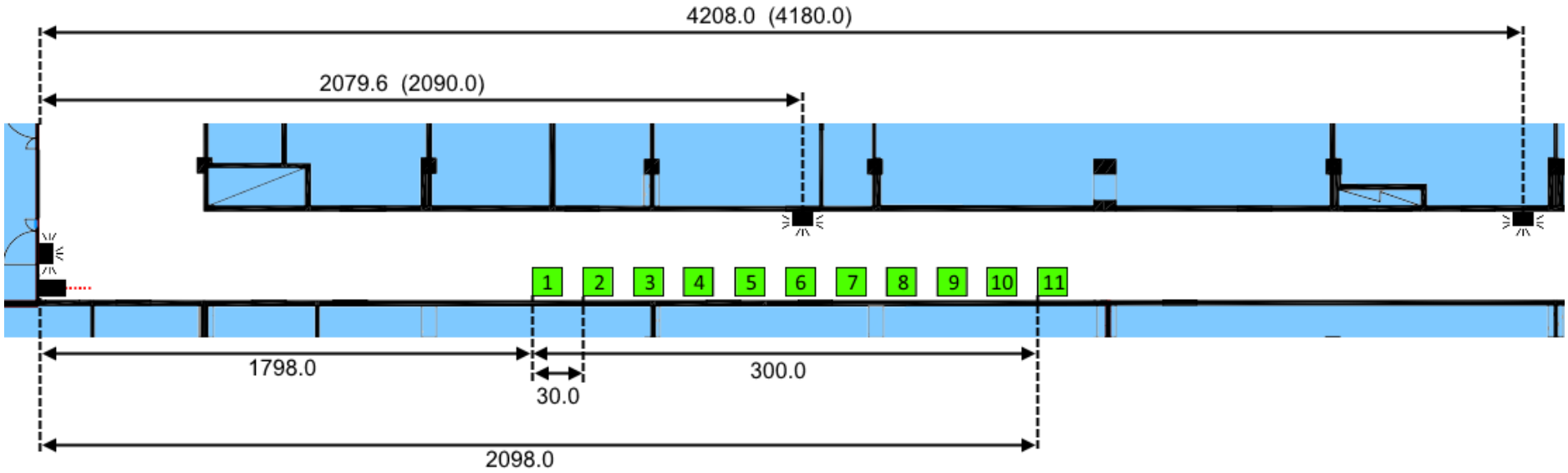

Figure 35. *The layout of the second positioning test.*

APPENDIX D: EXAMPLES OF MEASURED CSV-FILES

Table 3. *A sample of a data file containing measurements from BMI160 and BMM150 sensors.*

DATE	TIMESTAMP	ACC X	ACC Y	ACC Z	GYRO X	GYRO Y	GYRO Z	MAG X	MAG Y	MAG Z	RHALL
2017-11-09 08:38:50.847168	1.51021E+12	153	60	16378	-432	110	-65	345	-103	239	28641
2017-11-09 08:38:50.849683	1.51021E+12	-241	58	16123	-382	279	-110	345	-55	227	28645
2017-11-09 08:38:50.852207	1.51021E+12	-108	83	15952	-303	44	-73	393	-55	229	28641
2017-11-09 08:38:50.854720	1.51021E+12	-27	-41	15875	-318	41	-53	409	-71	221	28637
2017-11-09 08:38:50.857231	1.51021E+12	-173	109	16106	-208	51	-51	385	-55	231	28641
2017-11-09 08:38:50.859759	1.51021E+12	68	-87	16201	-291	-95	-66	377	-71	215	28641
2017-11-09 08:38:50.862259	1.51021E+12	34	15	16366	-306	81	-82	337	-23	207	28641
2017-11-09 08:38:50.864768	1.51021E+12	-243	227	16350	-289	202	-134	369	-95	217	28633
2017-11-09 08:38:50.867278	1.51021E+12	-41	132	16088	-353	-14	-114	369	-55	215	28637
2017-11-09 08:38:50.869783	1.51021E+12	157	279	16354	-399	129	-91	401	-71	221	28645
2017-11-09 08:38:50.872313	1.51021E+12	-7	381	17001	-478	269	-127	337	-15	223	28641

Table 4. *A sample of a data file containing measurements from BME280 sensor.*

DATE	TIMESTAMP	TEMP	PRES	HUM
2017-11-09 08:38:50.799218	1.51E+12	23.51	999.0483	33.96601
2017-11-09 08:38:50.836099	1.51E+12	23.51	999.0483	33.94395
2017-11-09 08:38:50.863795	1.51E+12	23.51	999.0326	34.275
2017-11-09 08:38:50.891380	1.51E+12	23.5	999.0069	34.04834
2017-11-09 08:38:50.919572	1.51E+12	23.5	999.066	33.85533
2017-11-09 08:38:50.946543	1.51E+12	23.5	999.0486	33.93235
2017-11-09 08:38:50.974242	1.51E+12	23.51	999.0244	33.81692
2017-11-09 08:38:51.001156	1.51E+12	23.5	999.0595	34.05937
2017-11-09 08:38:51.028784	1.51E+12	23.51	999.0441	33.94927
2017-11-09 08:38:51.056302	1.51E+12	23.51	999.0549	34.05424
2017-11-09 08:38:51.083961	1.51E+12	23.51	999.0089	33.91638

APPENDIX E: PLOTTED DATA FROM ELEVATOR TESTS

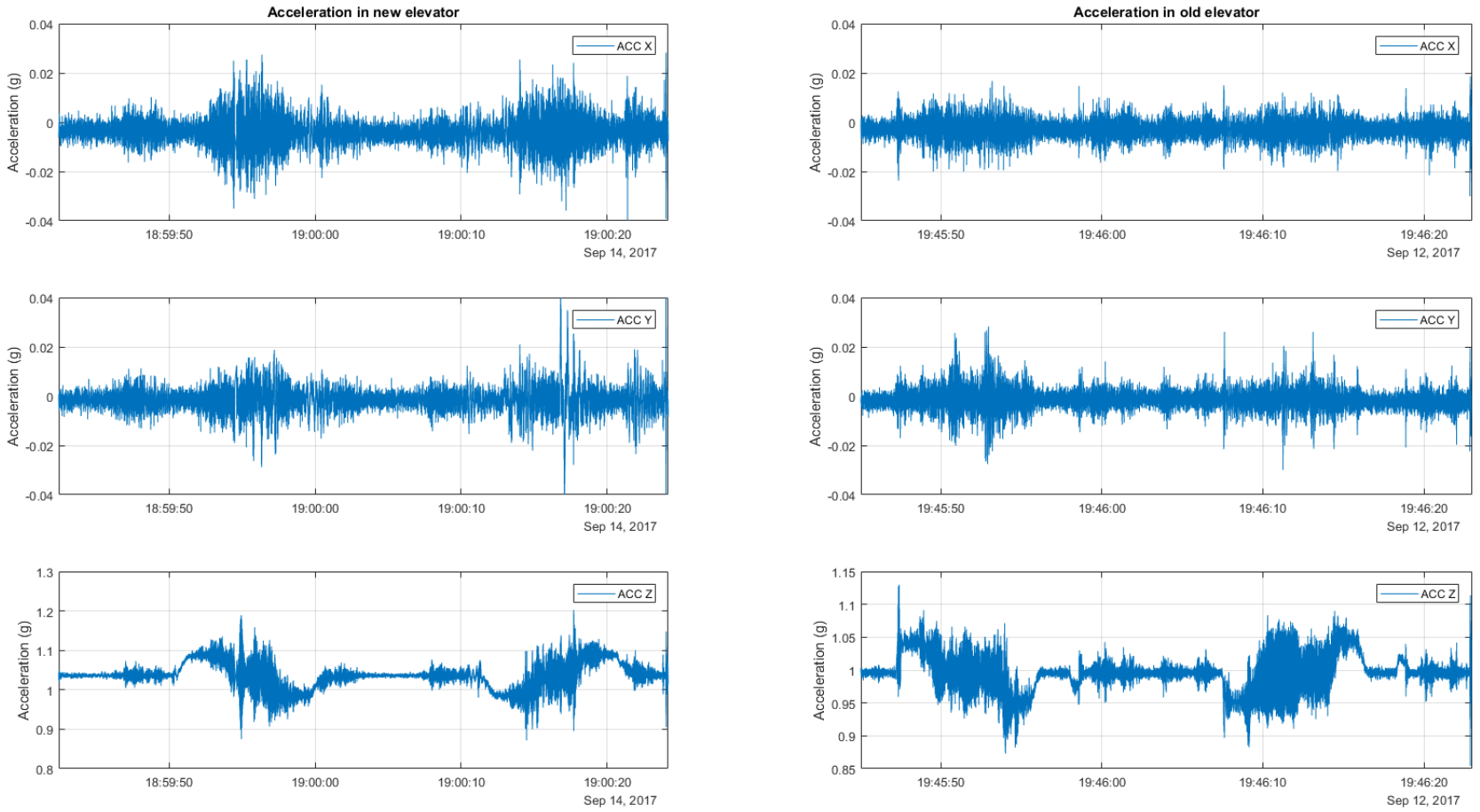

Figure 36. *The plotted acceleration data of the tested elevators.*

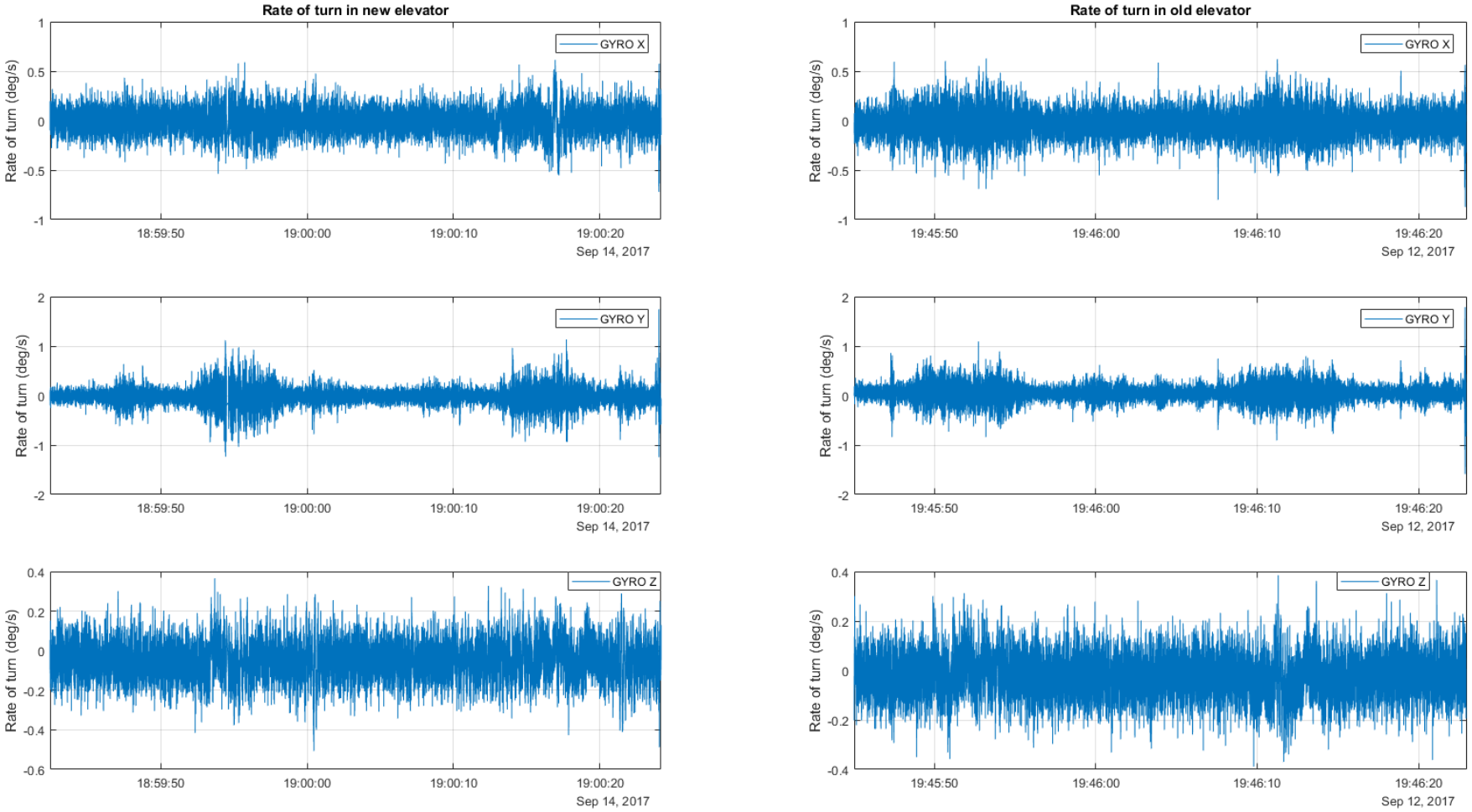

Figure 37. *The plotted gyroscope data of the tested elevators.*

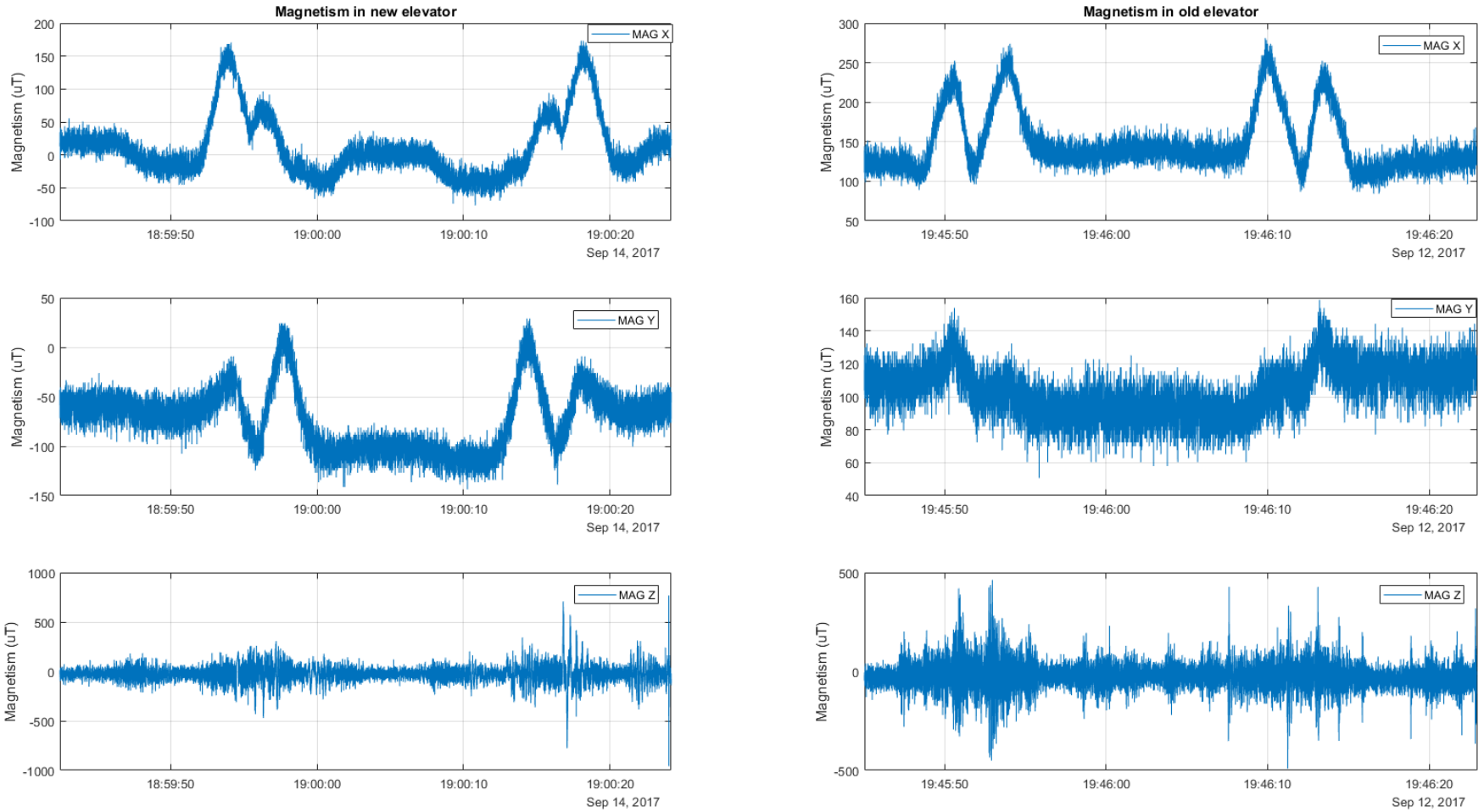

Figure 38. *The plotted magnetism data of the tested elevators.*

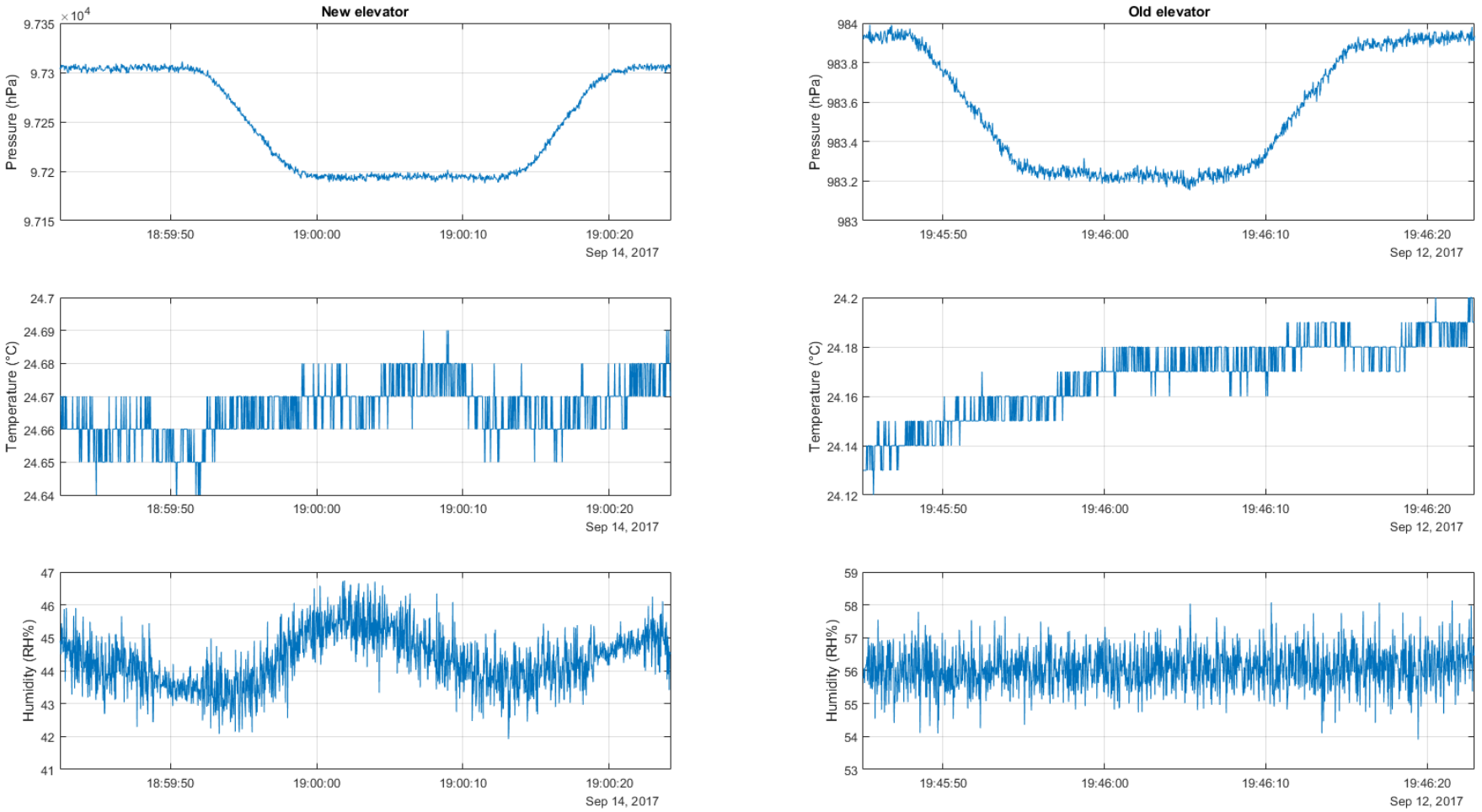

Figure 39. *The plotted environmental data of the tested elevators.*

APPENDIX F: THE RESULTS OF THE FIRST POSITIONING TEST

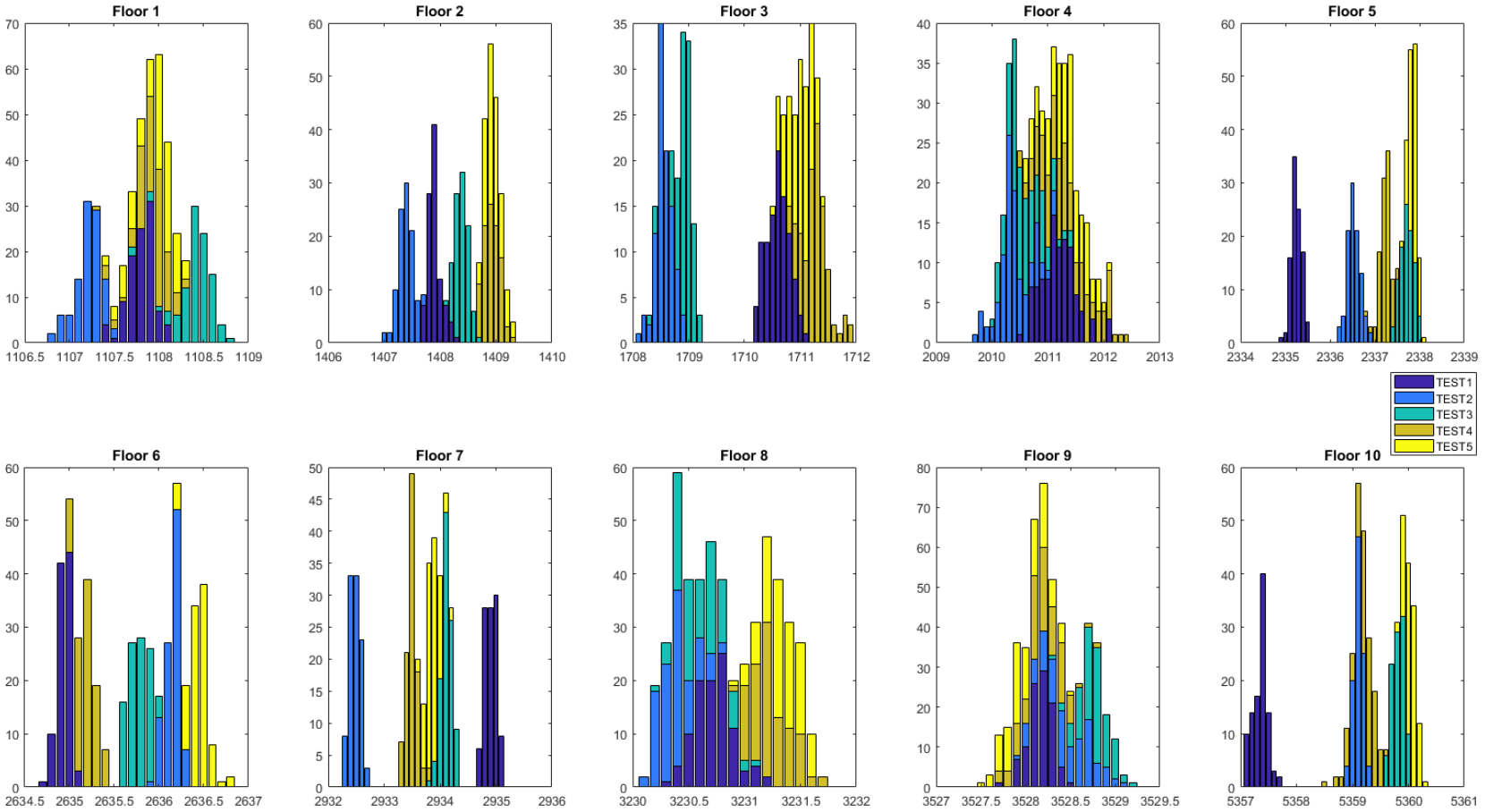

Figure 40. *All the position samples of the first positioning test.*

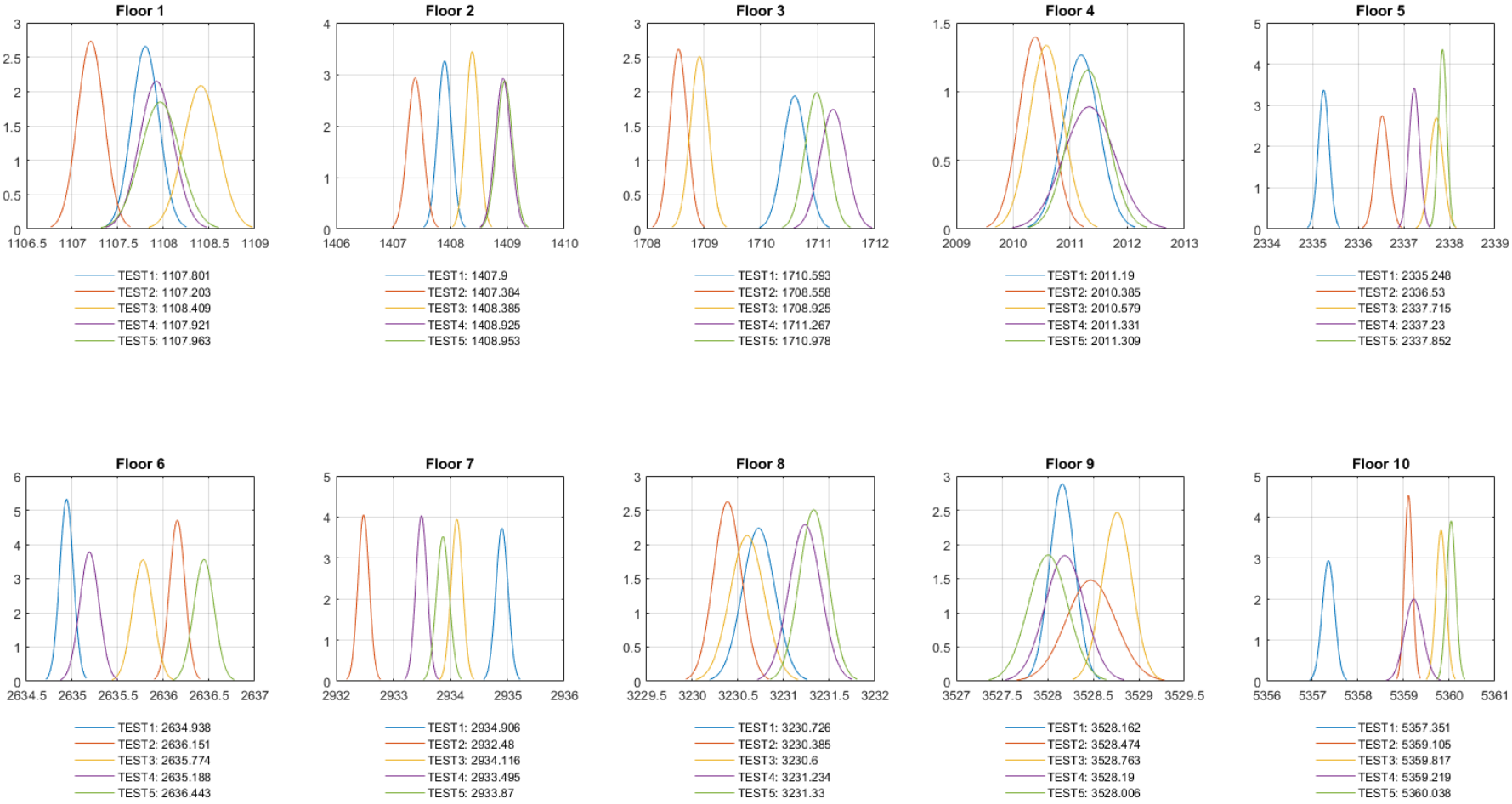

Figure 41. *The normal distributions and the averages of the measured position samples from the first positioning test.*

Table 5. *The calculated averages from the first positioning test.*

Floor	1	2	3	4	5	6	7	8	9	10	Average error per test
Test 1	1107.801	1407.9	1710.593	2011.19	2335.248	2634.938	2934.906	3230.726	3528.162	5357.351	
Test 2	1107.203	1407.384	1708.558	2010.385	2336.53	2636.151	2932.48	3230.385	3528.474	5359.105	
Error	-0.598	-0.516	-2.035	-0.805	+1.282	+1.213	-2.426	-0.341	+0.312	+1.754	1.128
Test 3	1108.409	1408.385	1708.925	2010.579	2337.715	2635.774	2934.116	3230.6	3528.763	5359.817	
Error	+0.608	+0.485	-1.668	-0.611	+2.467	+0.836	-0.790	-0.126	+0.601	+2.466	1.066
Test 4	1107.921	1408.925	1711.267	2011.331	2337.23	2635.188	2933.495	3231.234	3528.19	5359.219	
Error	+0.120	+1.025	+0.674	+0.141	+1.982	+0.250	-1.411	+0.508	+0.028	+1.868	0.801
Test 5	1107.963	1408.953	1710.978	2011.309	2337.852	2636.443	2933.87	3231.33	3528.006	5360.038	
Error	+0.162	+1.053	+0.385	+0.119	+2.604	+1.505	-1.036	+0.604	-0.156	+2.687	1.031
Average error per floor	0.372	0.770	1.191	0.419	2.084	0.951	1.416	0.395	0.274	2.194	1.006

APPENDIX G: THE RESULTS OF THE SECOND POSITIONING TEST

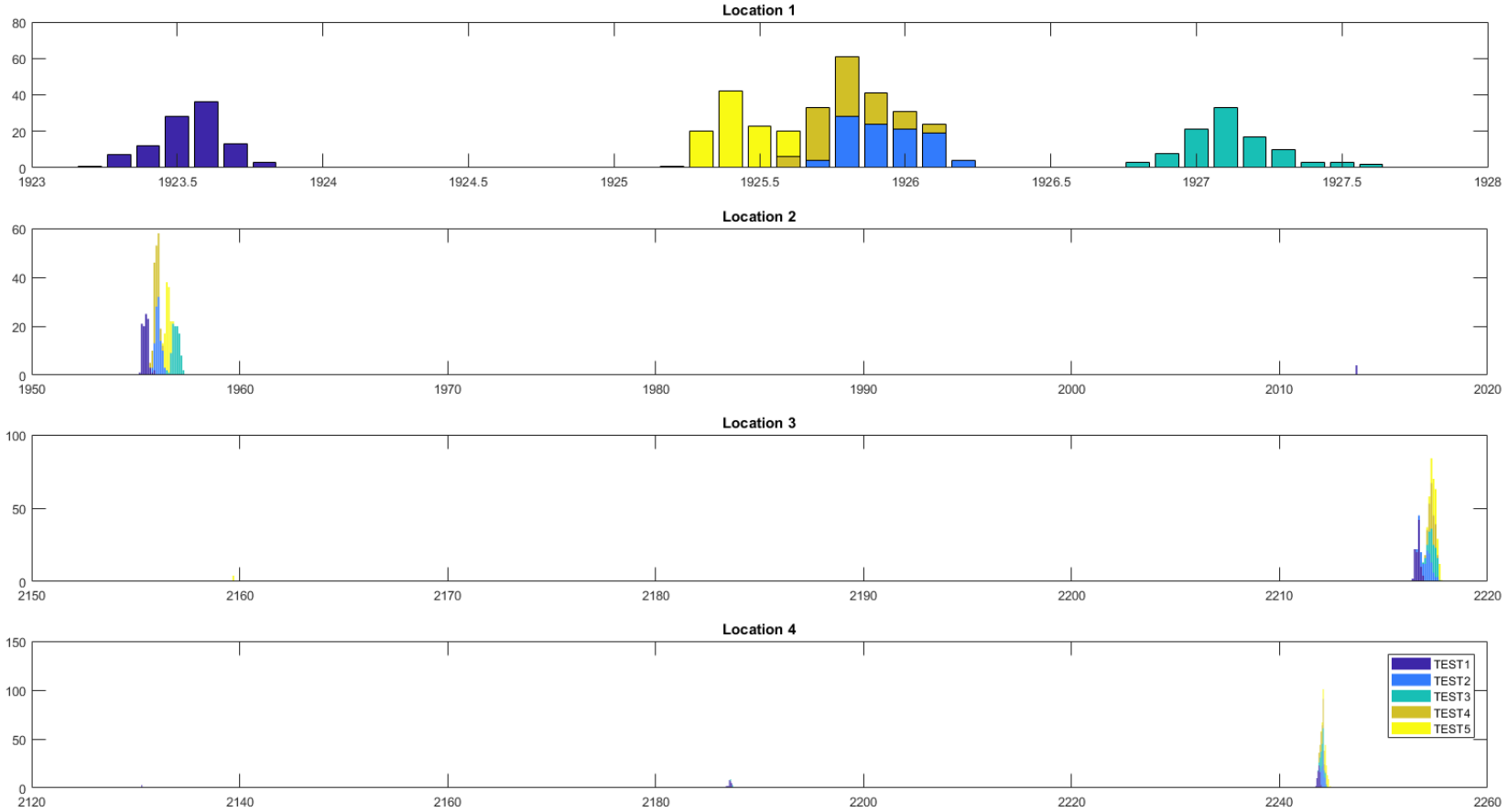

Figure 42. *The position samples of locations 1-4 of the second positioning test*

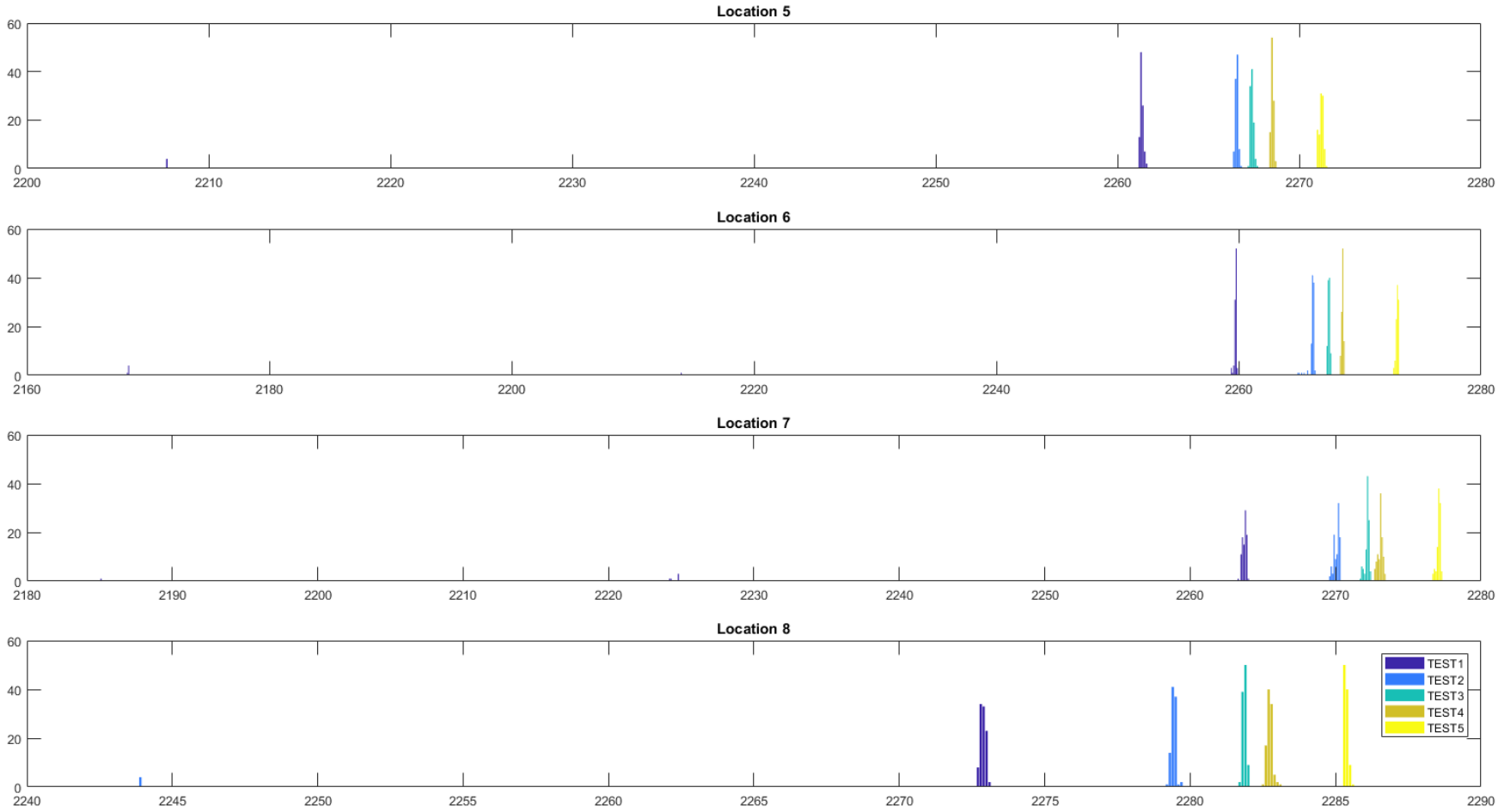

Figure 43. *The position samples of locations 5-8 of the second positioning test.*

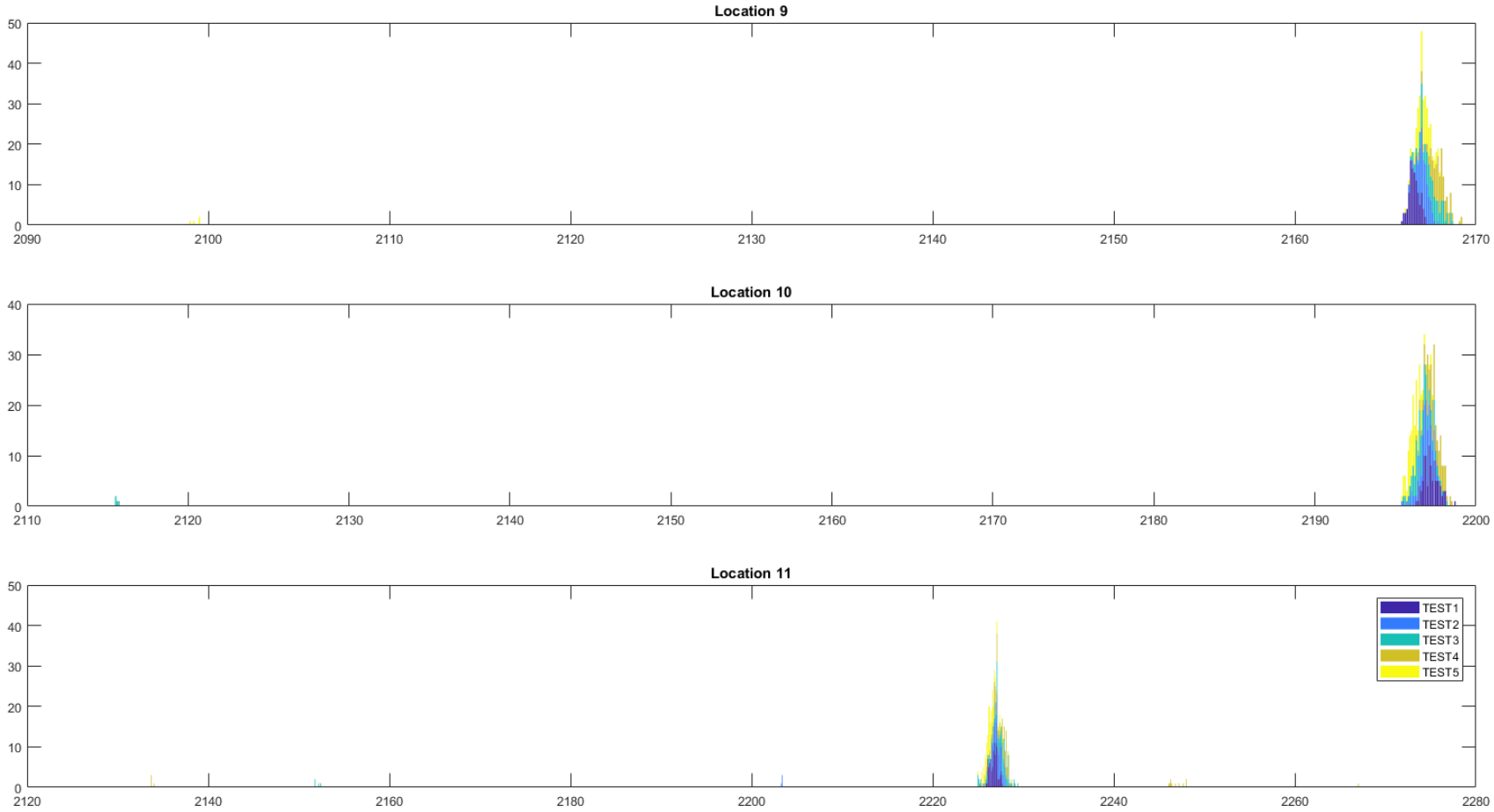

Figure 44. *The position samples of locations 9-11 of the second positioning test*

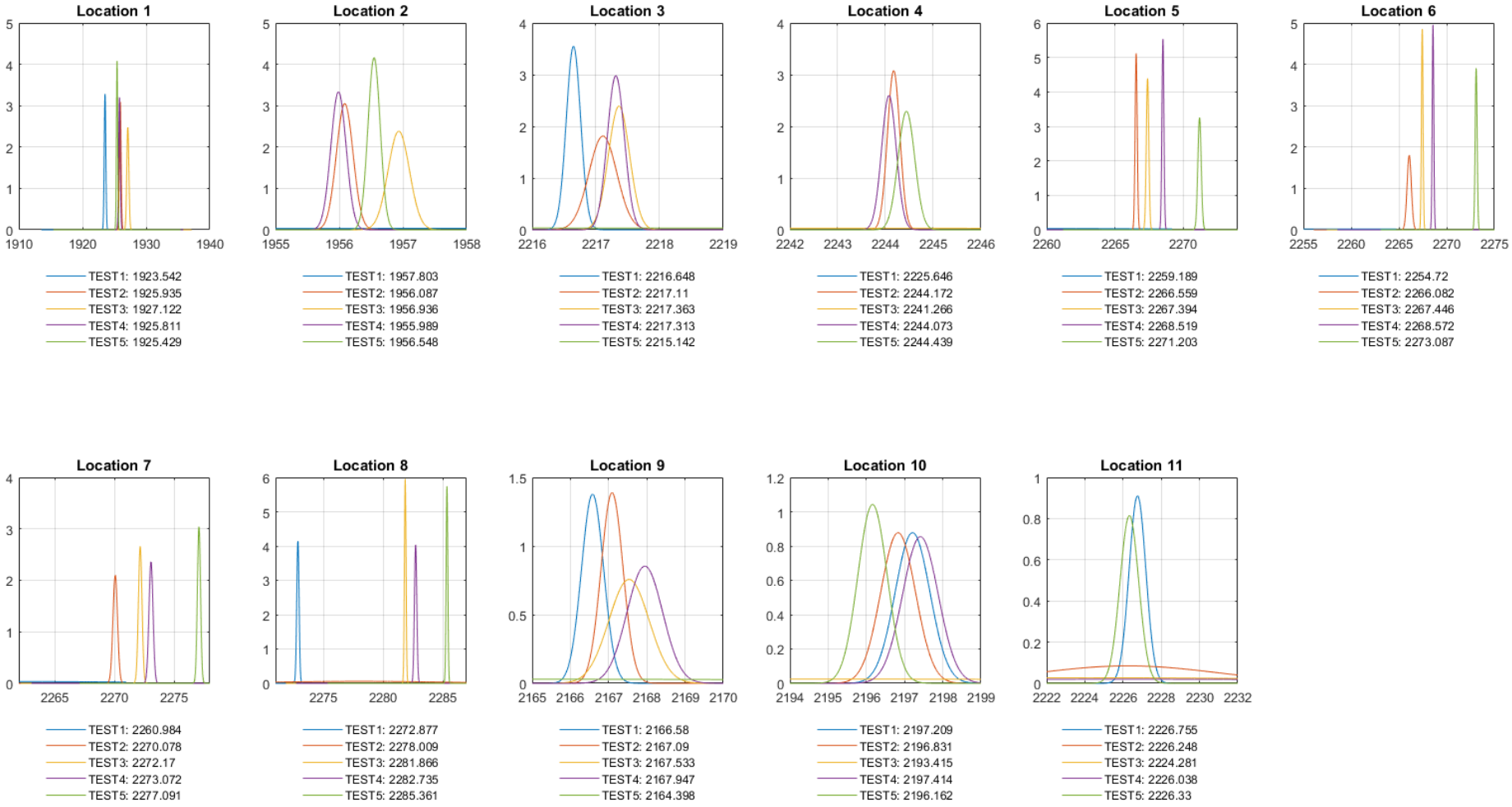

Figure 45. *The normal distributions and the averages of the measured position samples from the second positioning test.*

Table 6. *The calculated averages from the second positioning test.*

Location	1	2	3	4	5	6	7	8	9	10	11	Average error per test
Test 1	1923.542	1957.803	2216.648	2225.646	2259.189	2254.72	2260.984	2272.877	2166.58	2197.209	2226.755	
Test 2	1925.935	1956.087	2217.11	2244.172	2266.559	2266.082	2270.078	2278.009	2167.09	2196.831	2226.248	
Error	-2.393	+1.716	-0.462	-18.526	-7.37	-11.362	-9.094	-5.132	-0.510	+0.378	+0.507	5.223
Test 3	1927.122	1956.936	2217.363	2241.266	2267.394	2267.446	2272.17	2281.866	2167.533	2193.415	2224.281	
Error	-3.58	+0.867	-0.715	-15.62	-8.205	-12.726	-11.186	-8.989	-0.953	+3.794	+2.474	6.283
Test 4	1925.811	1955.989	2217.313	2244.073	2268.519	2268.572	2273.072	2282.735	2167.947	2197.414	2226.038	
Error	-2.269	+1.814	-0.665	-18.427	-9.33	-13.852	-12.088	-9.858	-1.367	-0.205	+0.717	6.417
Test 5	1925.429	1956.548	2215.142	2244.439	2271.203	2273.087	2277.091	2285.361	2164.398	2196.162	2226.33	
Error	-1.887	+1.255	+1.506	-18.793	-12.014	-18.367	-16.107	-12.484	+2.182	+1.047	+0.425	7.824
Average error per location	2.532	1.413	0.837	17.841	9.230	14.077	12.119	9.116	1.253	1.356	1.031	6.437

Table 7. *The comparison between test 1 results and the reference laser measures.*

Location	**1**	**2**	**3**	**4**	**5**	**6**	**7**	**8**	**9**	**10**	**11**
Laser	1798.0	1828.0	1858.0	1888.0	1918.0	1948.0	1978.0	2008.0	2038.0	2068.0	2098.0
Distance to previous location		+30.0	+30.0	+30.0	+30.0	+30.0	+30.0	+30.0	+30.0	+30.0	+30.0
Distance to location 1		30.0	60.0	90.0	120.0	150.0	180.0	210.0	240.0	270.0	300.0
Test 1	1923.542	1957.803	2216.648	2225.646	2259.189	2254.72	2260.984	2272.877	2166.58	2197.209	2226.755
Distance to previous location		+34.261	+258.845	+8.998	+33.543	-4.469	+6.264	+11.893	-106.297	+30.629	+29.546
Error		+4.261	+228.845	-21.002	+3.543	-34.469	-23.736	-18.107	-136.297	+0.629	-0.454
Distance to location 1		34.261	293.106	302.104	335.647	331.178	337.442	349.335	243.038	273.667	303.213
Error		+4.261	+233.106	+212.104	+215.647	+181.178	+157.442	+139.335	+3.038	+3.667	+3.213